Journal of Nuclear Materials 628 (2026) 156601

Contents lists available at ScienceDirect

Journal of Nuclear Materials

journal homepage: www.elsevier.com/locate/jnucmat

Effect of neutron irradiation on the fracture behaviour of tungsten fibre-reinforced tungsten composites

J. Riesch [a,*], A. Zinovev [b], E. Gaganidze [c], H. Ries [c], H. Gietl [a], Y. Mao [d], J. W. Coenen [d,e], T. Höschen [a], D. Terentyev [b,f], R. Neu [a,g]

[a] Max-Planck-Institut für Plasmaphysik, 85748 Garching, Germany
[b] Institute for Nuclear Energy Technology, Belgian Nuclear Research Center, SCK CEN, 2400, Mol, Belgium
[c] Karlsruhe Institute of Technology (KIT), Institute for Applied Materials, Hermann-von-Helmholtz-Platz 1, 76344 Eggenstein-Leopoldshafen, Germany
[d] Forschungszentrum Jülich GmbH, Institut für Energie- und Klimaforschung – Plasmaphysik, 52425 Jülich, Germany
[e] Department of Engineering Physics, University of Wisconsin - Madison, 53706, Madison, WI, USA
[f] Department of Materials, Textiles and Chemical Engineering, Ghent University, Technologiepark 46, B-9052, Zwijnaarde Belgium, Ghent, Belgium
[g] Technische Universität München, 85748 Garching, Germany

ARTICLE INFO

Keywords:
Tungsten
Wire
Composites
Neutron irradiation
Extrinsic toughening
Ductility

ABSTRACT

Tungsten features a unique combination of properties and is therefore the primary candidate for the most highly loaded components in future fusion power plants. However, tungsten suffers from an intrinsic brittleness at low temperature and is susceptible to operational embrittlement, meaning the degradation of material properties due to neutron irradiation will be a huge challenge. Tungsten fibre-reinforced tungsten composites overcome the intrinsic brittleness of tungsten by relying on extrinsic toughening mechanisms. The effect of neutron irradiation on these mechanisms has been an open question up to now. In this context the EUROfusion consortium launched an irradiation campaign at the Belgian reactor BR2 to study the effects of neutron irradiation on the mechanical properties of promising advanced materials including tungsten fibre-reinforced tungsten composites. In this campaign, bulk tungsten long fibre-reinforced tungsten composites produced by chemical vapour deposition and tungsten short fibre-reinforced tungsten composites produced by powder metallurgy have been irradiated for the first time under neutron irradiation. The samples have been irradiated up to 0.7–0.8 dpa at 600 °C and 1000 °C. 3-point bending tests on miniaturised notched samples showed that both materials retain toughness after irradiation. While the short fibre-reinforced powder metallurgical material shows a deterioration of properties, the chemically deposited material shows constant toughness after irradiation even at the lowest test temperature of 100 °C. The results reveal that extrinsic toughening in this material is resistant to irradiation embrittlement. Moreover, the reinforcing tungsten fibres show no sign of a reduction in ductility after irradiation. This is in contrast to results obtained for bulk tungsten, which typically suffers from significant irradiation hardening, and opens new design options.

1. Introduction

As tungsten features a unique property combination, it is currently the main candidate for the plasma facing material in future fusion reactors such as the European DEMO reactor [1–3]. In the last years many new material concepts have been developed to overcome the low temperature brittleness of tungsten [4–6] including, alloying, utilisation of ultra fine grained material and composite structures [7].

Tungsten fibre-reinforced tungsten composites (W_f/W) have been developed by combining the two later concepts. W_f/W consists of tungsten wire[1] with an engineered interface embedded into a tungsten matrix. The wire is produced by cold drawing and thus features an ultra fine grained microstructure as well as a high strength and ductility with a brittle to ductile transition already at -100 °C [8]. The matrix is produced by chemical vapour deposition (CVD) or powder metallurgy (PM) The CVD matrix is typically very dense with a few large range pores (see e.g. Wartacz et al. [9]), the PM matrix shows a randomly distributed porosity (see e.g. Mao et al. [10]). Thus, W_f/W produced by CVD can show large local quality variations whereas W_f/W produced by PM is typically more homogeneous. The fiber reinforcement can be either directionally aligned continuous long fibers or randomly oriented short fibers.

* Corresponding author.
E-mail address: johann.riesch@ipp.mpg.de (J. Riesch).

[1] If the wire is used within the composite it is named fibre in the following.

https://doi.org/10.1016/j.jnucmat.2026.156601
Received 16 September 2025; Received in revised form 13 March 2026; Accepted 17 March 2026
Available online 30 March 2026
0022-3115/© 2026 The Author(s). Published by Elsevier B.V. This is an open access article under the CC BY license (http://creativecommons.org/licenses/by/4.0/).

Compared to conventional tungsten, the main benefit of W_f/W is its high fracture toughness, even at room temperature (RT), due to extrinsic toughening mechanisms [11]. Similar to ceramic matrix composites, these mechanisms activate stress redistribution through local energy dissipation, thereby increasing the resistance to fracture [12,13]. Toughening is achieved when a growing crack interacts with the fibres in its wake. A key property is the interface between fibres and matrix, which enables debonding during crack propagation –a prerequisite for toughening– and maximizing energy consumption during crack opening [14]. The most effective mechanism is ductile fibre bridging, where fibres in the crack wake are plastically deformed during crack opening [15]. This plastic deformation dissipates energy and thereby increases the materials resistance to crack growth and thus its toughness. Especially in the long-fibre material the properties are dominated by this mechanism and thus by the fibre properties [16,17]. Other mechanisms like elastic bridging and fibre pull-out still allow toughening even if the W fibres embrittle [13]. Potassium doping is used to stabilize the microstructure of the W fibres against temperature induced recrystallisation and grain growth [18], stabilizing these key properties even at elevated temperature [11,19]. However, the W fibre is susceptible to embrittlement by small amounts of carbon [20,21].

Initial studies demonstrating that the toughening concept works have placed this material among the promising candidates for high-heat-flux applications in future fusion reactors [6,22]. In recent years, development efforts have focused on upscaling and on compatibility with the fusion environment [23]. The effect of neutron irradiation on W_f/W was identified as a critical knowledge gap very early on [22]. In particular, it is important to understand the effect of neutron irradiation on the interface between fibres and matrix. Modifications could have a significant impact on toughness, as reported for SiC_f/SiC [24]. The effects on the mechanical properties of the fibres are highly significant as well, since these strongly influence the behaviour of W_f/W. Although, fibres appear to retain their good mechanical behaviour during ion irradiation [25,26], this is not clear for neutron irradiation, where other effects could become active e.g. embrittlement by transmutation products.

Plasma-facing materials in the environment of an energy-producing fusion reactor are exposed to significant neutron irradiation originating from the D-T nuclear reaction [27]. In addition to transmutation, neutron irradiation induces lattice defects through atomic displacements (displacement damage). In general, this leads to embrittlement which can be seen by an increase in yield strength accompanied by a decrease of ductility [28]. In bcc metals like tungsten this can lead to a complete loss of ductility after neutron irradiation at high fluences. Gaganidze et al. [29] reported on a shift in the ductile to brittle transition temperature (DBTT) of more than 750 °C for polycrystalline tungsten of ITER specification after neutron irradiation to 1 dpa at 1000 °C. More recent studies have shown that some improvement of the resistance against irradiation damage could be achieved by microstructural refinement [30]. The neutron energy spectrum in a D-T fusion reaction reaches 14 MeV (see e.g. Gilbert and Sublet [31]). Currently there is no suitable facility that provides sufficiently large fluxes at these prototypical fusion neutron energies. Two methods are mainly used as alternatives for materials studies: irradiation by high-energy ions [32,33] and irradiation in fission reactors [34,35]

Ion beams allow control of irradiation parameters such as energies, dose rates and sample temperatures as well as fast iterations, both of which are very helpful in material development programs [36]. However, depending on the used ion species and energy only a very shallow penetration depth of a few nm to approximately 100 µm (for light ions) is possible [37]. This is a particular challenge for the study of bulk mechanical propertiesand especially important for composite materials like W_f/W, where the toughening mechanisms are active over length scales of several hundred micrometers (µm) and more. Details for the use of high-energy ions as a substitute for neutron irradiation are found here [28,38].

A huge benefit of irradiation in fission reactors is the possibility to irradiate larger structures. By using neutrons, the role of transmutation can be investigated and damage rates are closer to what is expected in a fusion reactor (see e.g. Vicente et al. [39]). However, the differences in the energy spectrum need to be considered with respect to damage accumulation and transmutation [40,41] (see Gietl et al. [42] for an overview).

For the next step reactors, like DEMO, or even more so for a fusion power plant, the requirement regarding irradiation stability will be significantly increased [43]. While the damage level at the end of lifetime for the ITER divertor will be ≈ 1 dpa in tungsten [44] it will reach up to 2 dpa in tungsten and 7 dpa for copper per full power year in DEMO [3]. This makes the materials response to irradiation with respect to thermal and physical properties an important task for the future development [30]. In this context the EUROfusion consortium[2] launched an irradiation campaign both for baseline materials (EUROFER, tungsten, and CuCrZr) and advanced materials' concepts [6]. A number of advanced materials were irradiated in the Belgian material test reactor (BR2) in two lots, one for copper based materials (Lot A) and one for tungsten based materials (Lot B). The first results of these investigations are reported by Terentyev et al. [30].

In the group of W materials, tungsten fibre-reinforced composite materials (W_f/W) have been irradiated up to 0.7-0.8 dpa at 600 °C and 1000 °C. The main ojective of this study was to investigate the effect of irradiation on the toughening mechanisms and to determine whether the toughness remains.

Fracture mechanical 3-point bending tests on notched KLST[3] type samples [45] were performed as they allow to asses this effect and have been frequently used for W_f/W in the past. As the properties of composites generally depend strongly on their architecture, representative composite structures were chosen to assess the basic behaviour. Both, tungsten long fibre-reinforced tungsten composites produced by chemical vapour deposition (L-W_f/W) and tungsten short fibre-reinforced tungsten composites produced by powder metallurgy (S-W_f/W) have been investigated. Commercial W material produced by Plansee according to the ITER specifications (ITER grade W produced by Plansee – IGP) was used as a reference material.

In this contribution, we present information about the materials, and the irradiation as well as the testing conditions. The results of fracture tests in combination with microscopy investigations of the fracture surfaces are presented both for non-irradiated and irradiated material. Finally, we discuss the implications of the results for the potential application of these composite materials in future fusion reactors.

2. Experimental

Long fibre- and short fibre-reinforced W_f/W were investigated. In both cases potassium doped W wire according to the chemical composition given in Table A.1 has been used as reinforcing fibres. L-W_f/W samples have been produced by layer-wise chemical vapour deposition as described by Riesch et al. [46]. In the CVD process, WF_6 is used together with H to form solid tungsten in a heterogeneous surface reaction on W wire weaves. The chemical composition of such a chemically deposited material is given in Table A.1.

For the weaves used in this study, warp wire with a diameter of 150 µm and a spacing of 200 µm is used together with weft wire with a diameter of 50 µm and a spacing of 2.5 mm. Details of the weave fabrication can be found in [47] (weave number 4). Due to the low weft wire density the composite properties are dominated by the warp wires and it can therefore be regarded as quasi-unidirectional. Prior to the CVD process the weaves were coated with a 1 µm thick Yttria layer by magnetron sputtering. The weaves were cleaned with isopropanol prior to

[2] https://euro-fusion.org/

[3] from the German "Kleinstprobe"

the reactive magnetron sputtering process. A 99.9 % pure yttrium target was used with the parameters given in [48]. The coating was performed in a two step deposition process with a interruption to turn the weaves similar to the procedure already used before [13,49].

To produce the composite, one of these weaves is placed on a heating table and the chemically deposited tungsten is grown into it until a desired thickness is reached. Then a second mesh is placed onto the infiltrated layer and the deposition is repeated. The steps are performed iteratively until the desired thickness is achieved. The deposition temperature was 600 °C leading to a deposition rate of 320 µm · h^{-1}. The deposition time for one layer was around 30 min. In-between each layer the reaction chamber was opened to place the next layer. This was done at a temperature of 250 °C as a compromise between processing time and minimizing oxidation. All layers are placed with the same orientation, leading to a main reinforcement parallel to the warp wire direction of the individual weaves. For the irradiation campaign and corresponding reference tests in non-irradiated condition, two identical plates were produced, each with 7 layer weaves and a size of 50 mm by 50 mm. The same process was used to produce a third plate for additional reference tests. After fabrication, some large cracks were detected on the plates parallel to the warp wire orientation. The samples were cut avoiding these cracks. Samples that looked best during visual inspection were chosen for irradiation. The density and fibre volume fraction of L-W$_f$/W has been determined in the non-irradiated condition for 4 specimens using cross-section pictures on polished samples in order to assess the overall quality of the material. The cross-sections were done at a location sufficiently far from the fracture surface to avoid being influenced by it, yet as close as possible to remain representative. The density varies between 96.6 % and 99.6 %. The fibre volume fraction ranges between 9 and 13 %.

For the production of S-W$_f$/W, field assisted sintering as described in [10] was used. Short fibres with a diameter of 150 µm and a length of 2.4 mm were coated with a 2 µm thick Yttria layer (the same process as described in [50] was used) and then mixed with pure W powder (powder size 5 µm). This mixture was consolidated in a graphite die by field assisted sintering. In this process the sample was heated up to 1900 °C (as measured in the punch by a pyrometer) with a heating rate of 200 °C/min. The holding time at 1900 °C was 4 min at a pressure of 60 MPa. Three disks with a diameter of 40 mm and a thickness of 5 mm were produced. The density was approximately 92 % (measured by Archimedes principle) with a fibre volume fraction of 30 %.

The IGP (ITER grade W produced by Plansee) reference samples were made of a forged and thermally stress relieved bar with a square cross-section of 36x36 mm^2 and a length of 480 mm at a purity of 99.97 %. The material features a needle like grain structure elongated in the forging direction and was used in various other studies before (see for details e.g. Gaganidze et al. [29], Wirtz et al. [51], Yin et al. [52], Gaganidze et al. [53]).

From the raw materials sub-size charpy V-notch samples of KLST type geometry with a nominal dimension of 3×4×27 mm^3 were produced according to appendix XI in ASTM E2248 [54]. The notch had a depth of 1.0 mm ± 0.1 mm with a opening angle of 60°. Samples prepared from the third L-W$_f$/W plate had a notch depth of 0.6 mm ± 0.1 mm and were tested only in the non-irradiated state. Details of the sample geometry are given in Fig. 1. The samples were processed using electrical discharge machining (EDM). To minimize surface roughness/cracks caused by EDM, reduced power (compared to the standard process) was used for the first cut, followed by sizing with a reduced cutting speed. No sizing was used for the notch to allow for easier crack initiation. Before cutting the L-W$_f$/W plates were ground to remove any unevenness caused by the fabrication process. After cutting the samples were cleaned in nitric acid to remove the debris from the EDM process. Eleven samples were cut from the first two L-W$_f$/W plates and nine samples from the third plate. From each S-W$_f$/W disk eight samples were fabricated. In Fig. B.1 the cutting schemes of the plates and disks are given. For the L-W$_f$/W material the samples were oriented in a way that the fibres were parallel

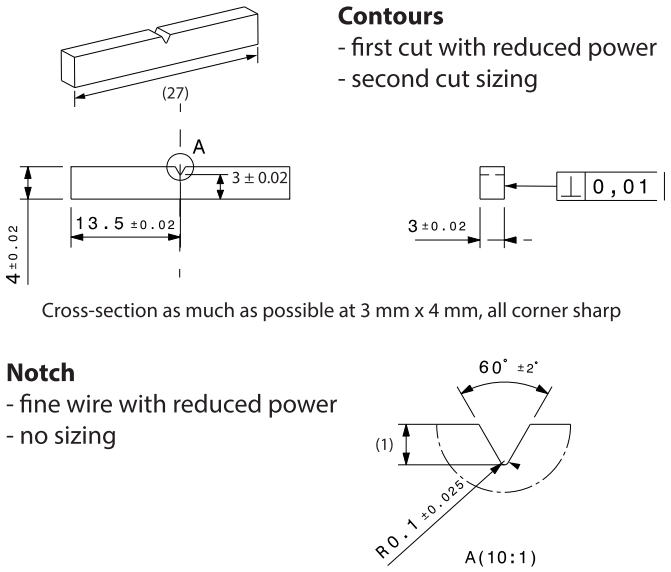

Fig. 1. Geometry of KLST type samples and details of parameters for electrical discharge machining.

to the long side. The samples were cut avoiding the large cracks on the plates (see above). In addition, three L-W$_f$/W samples were used from a previous fabrication campaign (see Gietl et al. [49]). EDM was also used to cut the IGP specimens from the bar in L-T orientation (as defined in ASTM E399). Twelve samples were irradiated for each composite type and eight samples for IGP. These samples were cleaned in an ultrasonic bath before being placed into the irradiation capsules. The remaining samples were used for reference tests in the non-irradiated condition.

Neutron irradiation was performed in BR2 for 167 days inside the fuel element in the position close to the centre of the reactor and in the midplane[4]. This position has an average fast neutron ($E > 1$ MeV) flux of 1×10^{14} n/m^2/s at a reactor power of 60 MW. The samples were encapsulated in a stainless steel tube with 1.5 mm wall thickness filled with He and Ne. Within the tubes the samples were held by holders made of Ti for lower and of W for higher irradiation temperature. The gap between the samples and the pressure tube was adjusted to achieve the desired target temperature during the irradiation following thermal and neutronic calculations. According to a finite element analysis of the thermal flow, variation of 25 – 50 °C occurred during the irradiation cycle (the lower the absolute irradiation temperature, the lower its in-cycle variation) due to the burnup of the fuel element.

The irradiation dose is calculated in displacement per atom (dpa) units using the MCNPX 2.7.0 code [55] with the threshold displacement energy of 55 eV, following the experimental data in [56,57] and in a similar way as described in [30]. Besides the value of 55 eV, other values for the threshold displacement energy (TDE) in tungsten were reported recently, namely: 90 eV [58,59] or 70 eV [60]. The currently reported dpa values can be re-calculated for another TDE by linear rescaling using a factor 55/TDE$_{new}$. The irradiation doses were determined to be 0.7 dpa from 6.23×10^{20} n/cm^2, $E > 1$ MeV and 2.3×10^{21} n/cm^2, $E < 1$ MeVat 600 °C and 0.8 dpa from 7.12×10^{20} n/cm^2, $E > 1$ MeV and 2.6×10^{21} n/cm^2, $E < 1$ MeVat 1000 °C using the MCNP calculations (accounting for neutron flux, gamma flux, heat release due to prompt and delayed gamma and neutron heating), reactor power measurements, and finite element thermal calculations. The irradiation temperatures are nominal values calculated as average during the cycle. Transmutation is reduced due to the stainless steel capsules and by choosing a position in the fuel channel where the highest fraction of fast neutrons occur. The

[4] RH basket with capsules in the centre tube of a standard fuel element

Table 1
Overview of performed tests. The first column gives the material and the following ones the state of the material. For each state the number of performed tests and the range of test temperatures are given.

Material	*Non-irradiated*	*Irradiated at* 600 °C	*Irradiated at* 1000 °C
IGP W	6 tests at 150 – 600 °C	3 test at 580–1200 °C	3 test at 580–1150 °C
L-W_f/W	11 tests at RT – 1000 °C	5 tests at 100 – 600 °C	5 tests at 100 – 1000 °C
S-W_f/W	5 tests at RT – 600 °C	5 tests at 100 – 600 °C	5 tests at 100 – 1000 °C

transmutation of Re and Os was calculated as described in [30]. Most of Re transmutation was expected to be close to the surface due to self shielding. The ALEPH code developed at SCK CEN [61] and publicly available nuclear databases [59,62,63] are used for the calculation of transmuted elements. The transmutation rate has then been calculated as a ratio of end dpa divided by total concentration of transmuted Re or Os. It was determined to be ~ 1.8 - 2 at.% Re dpa and ~ 0.2 at.% Os dpa which is in the range expected in a fusion power plant after one year [31]. No other elements were evaluated as Re and Os are the main transmutant elements of W. Six samples of each composite type and four samples of IGP W were irradiated for each condition. Altogether 4 capsules with 8 samples each were irradiated in one reactor cycle.

The post irradiation analysis was done in the material test laboratory of the Belgian Nuclear Research Center (SCK CEN) for tests up to a temperature of 600 °C and the Fusion Materials Laboratory (FML) at the Karlsruher Insitute for Technology (KIT) for high temperature tests up to 1200 °C. 3-point bending tests were performed according to ASTM E399 [64] .

At SCK CEN, an Instron servo-hydraulic universal testing machine equipped with an environmental chamber was used, which undergoes regular qualification and calibration procedures according to Belgian accreditation rules (BELAC). The machine and chamber were placed in a hot cell. Sample deflection was measured by the pull rod displacement, and the force was measured by a load cell with a maximum capacity of 100 kN. Both systems were calibrated prior to testing. The tests were performed in a displacement controlled mode with a constant cross-head speed of $0.2\,\mathrm{mm}\cdot\mathrm{min}^{-1}$. The span size was 18 mm and the tests were performed in air. The cross-head speed was chosen to equalize the deformation rate (in the tensile region of the sample) with the strain rate of tensile samples from the same irradiation campaign (see Terentyev et al. [30]). The load as well as the displacement of the central indenter were measured to assess force-displacement curves.

The FML system was a servo electric testing machine from Zwick located in a hot cell and equipped with a 10 kN load cell and a high temperature vacuum furnace (pressure 6×10^{-3} Pa). The tests were performed in a cross-head displacement controlled way with a deflection rate of $2\,\mu\mathrm{m}\cdot\mathrm{s}^{-1}$ and a span size of 25 mm. Displacement is reported as cross-head displacement.

Composite samples in non-irradiated condition were tested from RT up to 1000 °C while irradiated samples were tested from 100 °C up to 1000 °C. The IGP W was tested from RT up to 600 °C in non-irradiated condition and up to 1200 °C after irradiation. Table 1 gives an overview of the performed tests. In Appenix C the procedure for data visualisation is presented.

The broken half pieces of the tensile samples tested at SCK CEN were investigated by scanning electron microscopy (SEM). The samples were wiped with paper towels, and if necessary cleaned in an ultra-sonic bath before they were brought into the hot cell. All SEM images presented in this work were acquired using a secondary electron (SE) detector on a JEOL JSM-7100LV (JEOL, Tokyo, Japan) microscope. The operating conditions were: 20 kV accelerating voltage and a working distance between 12 and 20 mm. Optical imaging was done on fracture surfaces after bending testing at FML. The diameter of the broken fibres was determined as a measure of ductility for samples that were subjected to SEM microscopy. This was done for all fibers that exhibited ductile fracture.

3. Results

The force-displacement curves of IGP W are shown in Fig. 2 . In the as fabricated case, samples tested up to 350 °C show only elastic loading followed by a large load drop. For samples tested at 450 °C and above a significant displacement is seen after elastic loading. Only elastic deformation is observed after irradiation up to a testing temperature of 590 °C ± 10 °C regardless of the irradiation temperature. The maximum force withstood by the irradiated samples show a variation typical for brittle fracture. The displacement until fracture is similar for both irradiation temperatures. At a testing temperature of 1000 °C and above, plastic deformation follows elastic loading.

In Fig. 3 the fracture surfaces of irradiated samples tested at 590 °C ± 10 °C are shown. The fracture is dominated by cleavage. However, although showing no ductility in the force-displacement behaviour, there are some signs of ductile deformation in the fracture surface (see red arrows in Fig. 3 (b,d)). Overall the fracture surface shows some waviness which, however, does not influence the mechanical behaviour. There are signs of oxidation due to testing in air (see red circles in Fig. 3 (b,d)).

In Fig. 4 the stress-strain curves for S-W_f/W samples are shown. Non-irradiated material tested at RT shows a full drop in load with no additional displacement after elastic loading. At a testing temperature of 100 °C and above this behaviour changes and there is a more gentle decrease in load after reaching the maximum value. The maximum load and thus the fracture strength shows a strong variation and is highest for a testing temperature of 100 °C. The deviation from purely elastic behaviour at 100 °C corresponds with an onset of ductile deformation in the composite fibres. The ductile deformation is shown in Fig. 5 (b,d) in detail for the testing temperature of 100 °C and 580 °C. There is no obvious change with increasing temperature.

In the irradiated case the change in fracture behaviour from purely elastic occurs at different temperatures. In the case of an irradiation temperature of 600 °C this occurs at 300 °C and in the case of an irradiation temperature of 1000 °C it occurs at 580 °C (see Fig. 4). Similar to the non-irradiated state, this corresponds with a change in fracture behaviour of the fibres which starts for the lower irradiation temperature to become ductile at a testing temperature of 300 °C (see Fig. 6 (b)). At this temperature the sample irradiated at 1000 °C shows a fully brittle fracture (see Fig. 6 (d)). For this irradiation temperature very few individual fibres show observable ductility at a testing temperature of 450 °C. At a testing temperature of 580 °C the fracture surface seems to be more structured with visible fibres but a clear identification of ductile fibre deformation is not possible. The matrix is very similar for both irradiation temperatures: grain boundary failure up to a testing temperature of 450 °C and cleavage at 580 °C.

In Fig. 8, the force-displacement curves for L-W_f/W in the non-irradiated state are shown in comparison to irradiated state. For all temperatures, the curves for the non-irradiated material show a decrease in the slope after elastic loading similar to ductile materials. For most of the samples, this continues until the maximum load is reached, after which there is a gradual decrease featuring some step-wise drops. Some samples show a large and steep drop in load (without displacement) right at the end of elastic loading or until reaching maximum load before showing a gentle decrease.

In Fig. 7, the fracture surfaces for non-irradiated samples tested at 100 °C and 580 °C are shown. All fibres show ductile fracture. This is representative for all non-irradiated L-W_f/W samples. The fibres show necking and in most cases a knife-edge fracture. Only three single fibres show necking followed by cleavage fracture beyond the neck leading to an hour glass like structure (see Terentyev et al. [65] for comparison). The necking, i.e., the reduction in diameter, increases as the test temperature rises (compare (b) and (d) in Fig. 7). The values for the reduced diameter for each temperature are given in Table 2. The matrix shows cleavage fracture for all test temperatures.

In the irradiated case the force-displacement curves look very similar for all samples (see Fig. 8) and very similar to the non-irradiated

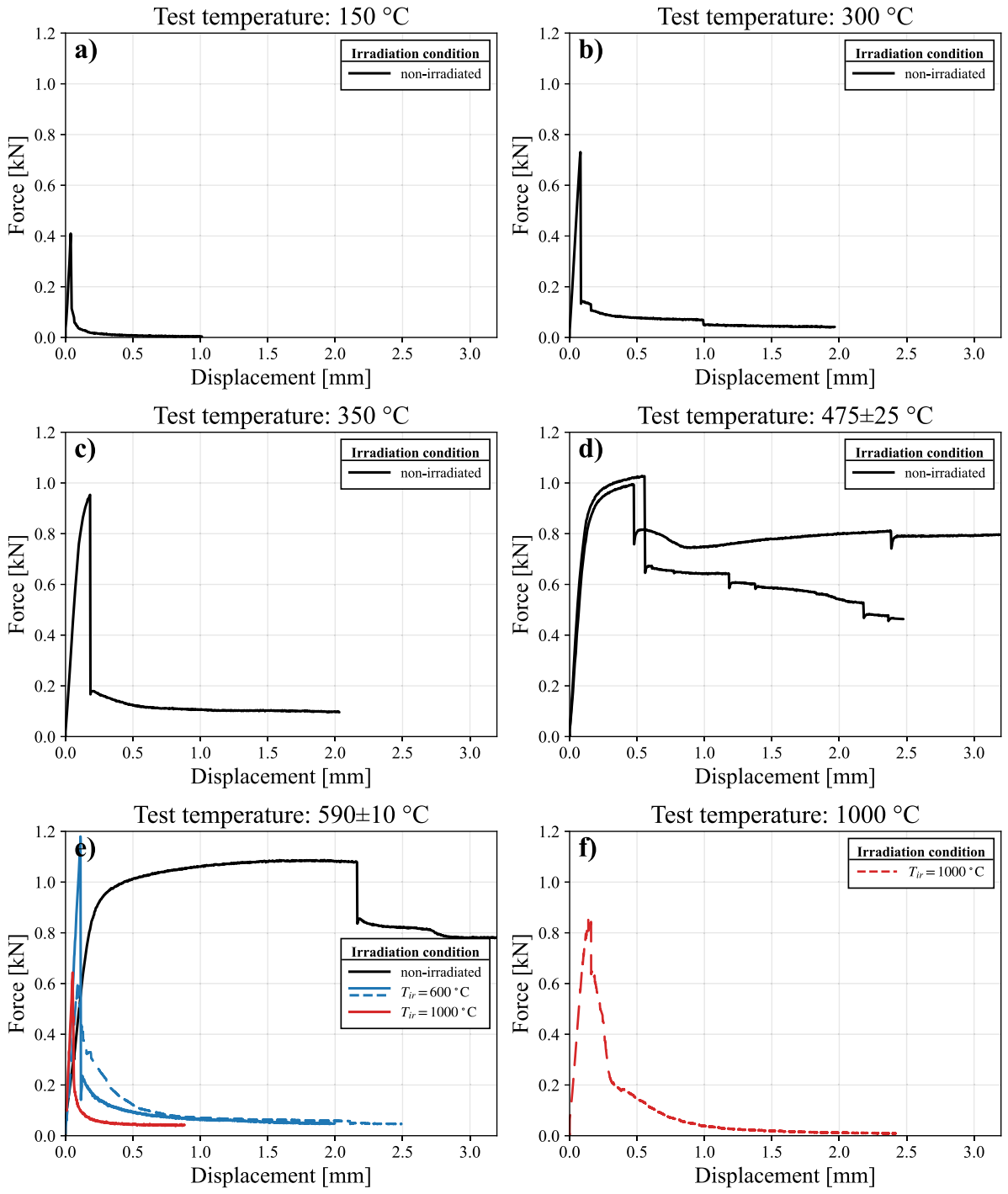

Fig. 2. Force-displacement curves of IGP W before and after irradiation for different test temperatures. Black lines show non-irradiated material. Blue lines represents samples irradiated at 600 °C, red lines samples irradiated at 1000 °C. The span was 18 mm for tests up to 475 °C ± 25 °C (solid lines) and 25 mm for tests at 1000 °C (dashed lines). For tests at 590 °C ± 10 °C both spans were used. . (For interpretation of the references to colour in this figure legend, the reader is referred to the web version of this article.)

case (no steep load drop). After a linear increase the slope decreases until reaching a maximum load value. Maximum load of irradiated samples is mostly similar to non-irradiated samples. At higher temperatures some non-irradiated samples show a higher maximum load. For irradiated material the maximum occurs at a lower displacement compared to the non-irradiated state. This is followed by a step-wise and gentle decrease in the load. Samples featuring different irradiation temperatures show similar displacement values but the maximum load is in all cases higher for an irradiation temperature of 1000 °C. Also in the irradiated case, almost all fibres show ductile deformation for all testing temperatures (see Fig. 9). Single fibres show both ductile deformation and brittle fracture. These fibres are concentrated in a region opposite to the artificial notch. All fibres featuring ductile deformation and ductile fracture show a significant reduction in diameter due to necking (see Table 2). Different to the non-irradiated state the change in the reduction in diameter with changing test temperature is not pronounced.

Table 2
Overview of reduced fibre diameter after fracture for non-irradiated and irradiated L-W_f/W samples. More than 30 fibres were evaluated for each condition. In the bottom row values for tests on the individual W-fibre (not within the composite) as determined in [19] are given for comparison.

	Reduced diameter [µm]	*Reduced diameter* [µm]	*Reduced diameter* [µm]	*Reduced diameter* [µm]	*Reduced diameter* [µm]	*Reduced diameter* [µm]
test temperature	*RT*	100 °C	300 °C	450 °C	500 °C	590 °C ± 10 °C
non-irradiated	112 ± 3	104 ± 6	92 ± 5	–	82 ± 5	78 ± 6
irradiated at 600 °C	–	95 ± 2	84 ± 2	84 ± 3	–	89 ± 2
irradiated at 1000 °C	–	105 ± 2	89 ± 2	85 ± 3	–	90 ± 3
W-fibre [19]	105	101	81	–	66	63

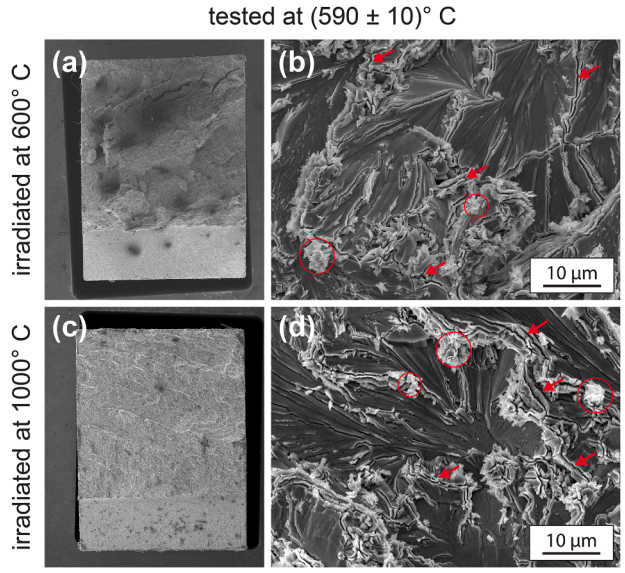

Fig. 3. Fracture surfaces of pure W samples which were irradiated at 600 °C (a,b) and 1000 °C (c,d) and tested at 590 °C ± 10 °C. On the left an overview picture is shown (sample size 3 mm x 4 mm). On the right a representative magnification of the fracture surface is shown. The fracture is dominated by cleavage but there are indications of ductile deformation some of which are exemplified by red arrows. Flower-like structures on sharp edges indicate oxidation (highlighted by red circles). (For interpretation of the references to colour in this figure legend, the reader is referred to the web version of this article.)

There is no significant difference between the two irradiation temperatures. In all cases the matrix shows cleavage fracture. For the higher testing temperatures only optical images are available. Nevertheless, a dominating ductile deformation of the fibres is also obvious at these temperatures.

4. Discussion

4.1. Measuring technique

In neutron irradiation experiments sample size is usually reduced to minimize irradiation volume and maximize number of samples. Nevertheless, sample numbers are typically low due to restricted space. This complicates quantitative measurements, especially if brittle fracture occurs. KLST type samples used in this study allow, due to their small size, for an adequate number of samples and have already been used frequently to evaluate the properties of W_f/W [12,13]. Similar to previous studies 3-point bending tests on these samples allow an assessment of the toughening effect and its active mechanisms. As long as sample geometries and fibre volume fractions are similar, a quantitative comparison is possible, although size effects are known to be pronounced in these materials [17]. This allows for a comparison in-between the tested material groups and to other studies on W_f/W-composites to assess the effect of irradiation.

The presented mechanical tests were performed on two different systems featuring a different testing span of 18 mm (SCK CEN) and 25 mm (KIT) respectively. The differences in the testing span lead to a different stress at the crack tip under a similar load (assuming other geometries are similar). This means that, at crack initiation, the same bending force on test specimens with a larger span results in a 40 % higher stress at the crack tip than on test specimens with a smaller span. Since the geometric dependencies change during crack propagation this correlation is only possible for crack initiation. However, for L-W_f/W samples tested at 590 °C ± 10 °C there are samples featuring a different test span but show an almost similar curve. This indicates that at least a qualitative comparison between the results of the two testing systems is possible.

Given the experimental constraints described above we performed the following approach. We used the force-displacement behaviour to qualitatively evaluate toughness, i.e. to determine whether extrinsic toughening mechanisms are active in the composite materials. Investigation of the fracture surface is used to determine the type of active mechanisms. As crack lengths were not measured we calculate the fracture energy instead of fracture toughness[5] for a quantitative comparison. We use the integral of the force-displacement curve between the first onset of failure after elastic loading and a load drop to a quarter of the maximum load.

In the case of ductile fibre fracture the reduction in diameter allows a quantitative assessment of the irradiation effect on ductility of the fibre. Since a sample contains up to 48 fibers, the results are statistically relevant despite the limited number of samples. As diameter reduction has been frequently used as a measure for fibre ductility in studies on individual fibres [19] and W_f/W composites [49], correlation to previous studies is possible.

4.2. Irradiation effect on fracture behaviour and toughness

For a classification of the fracture toughness and its change due to irradiation the fracture energy as the integral of force over displacement was calculated for each sample (see Fig. 10 and Table E.1). Samples with a smaller notch depth of 0.6 mm and thus a larger fracture area are indicated by (*) and shown as open symbols. This has to be taken into account, as samples with similar fracture properties but a larger area would also show a larger fracture energy. Fracture energy in combination with the force-displacement behaviour and the examination of the fracture surfaces makes it possible to evaluate the effect of irradiation on the toughness of W_f/W. In the following, a detailed discussion is given for each material, and the results are summarized in Table D.1.

The fracture energy of the non-irradiated *IGP-W* is negligible below 300 °C and increases significantly above this temperature. For irradiated material, this transition happens at 1000 °C, with the transition from purely elastic to ductile behaviour being observed in the force-displacement curve (see Fig. 2). This marks the DBTT. The shift of about

[5] as defined in ASTM E399 [64]

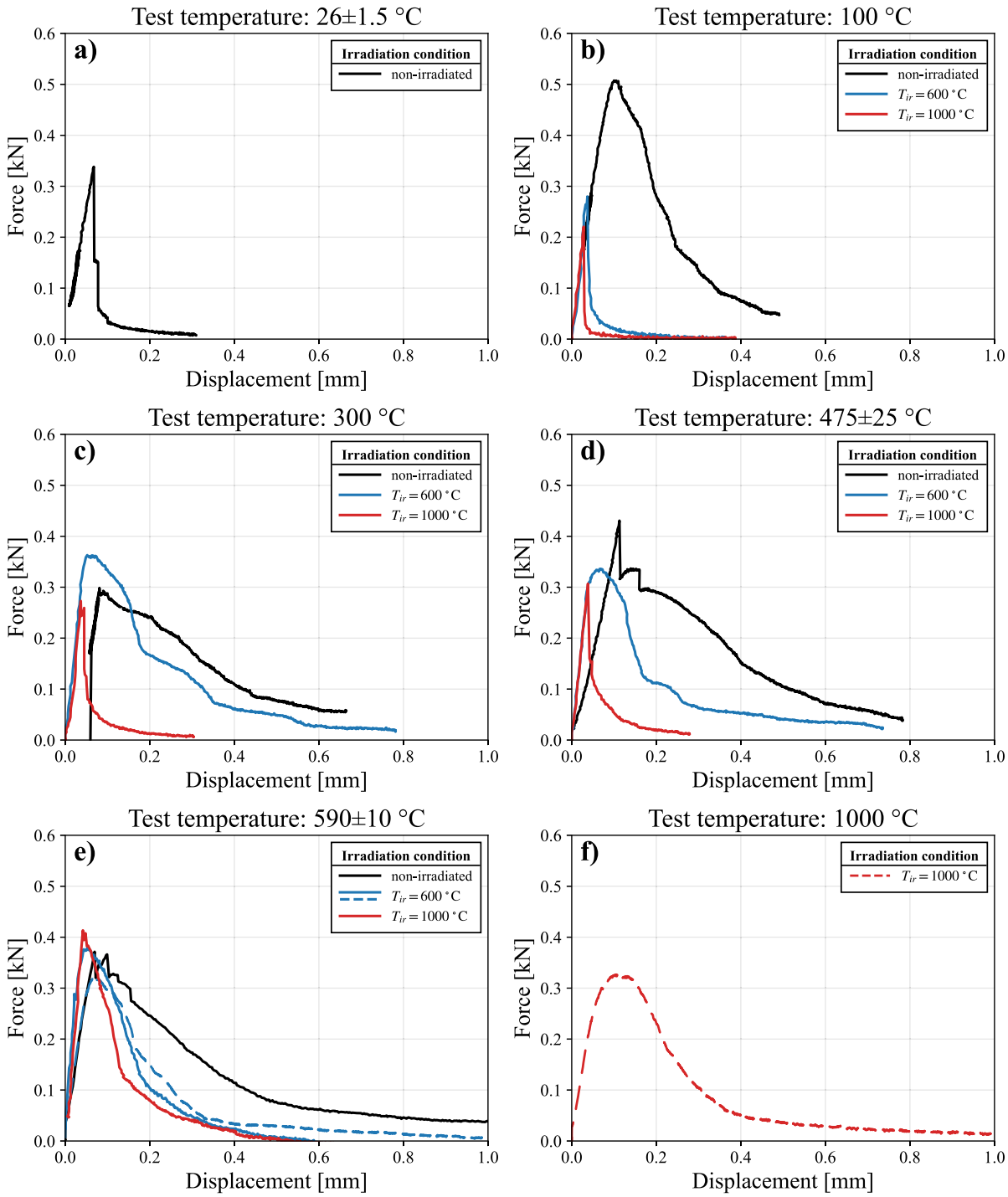

Fig. 4. Force-displacement curves of S-W_f/W before and after irradiation for different test temperatures. Black lines show non-irradiated material. Blue lines represents samples irradiated at 600 °C, red lines samples irradiated at 1000 °C. The span was 18 mm for tests up to 475 °C ± 25 °C (solid lines) and 25 mm for tests at 1000 °C (dashed lines). For tests at 590 °C ± 10 °C both spans were used. (For interpretation of the references to colour in this figure legend, the reader is referred to the web version of this article.)

600 °C is consistent with the values reported in literature [29,53]. The reduced absolute temperatures observed in comparison to literature values are attributed to the different sample orientation (elongated grains perpendicular to crack direction).

In the case of *S*-W_f/W, toughness (defined by an increase in the fracture energy) is observed at a temperature of 100 °C and above. The observed ductile deformation of the fibres indicates that the dominating mechanism is the ductile crack bridging. In the irradiated case this onset of toughening is dependent on the irradiation temperature - for samples irradiated at 600 °C it occured at a testing temperature of 300 °C, for samples irradiated at 1000 °C at a testing temperature of 590 °C ± 10 °C. Whereas for an irradiation temperature of 600 °C also ductile fibre bridging seems to occur this is not clear for the higher irradiation temperature. In this case, the fracture surface with some protruding fibres indicates that pull out may play a role. Looking at the fracture energy the gain in toughness is much smaller compared to the ductile deformation

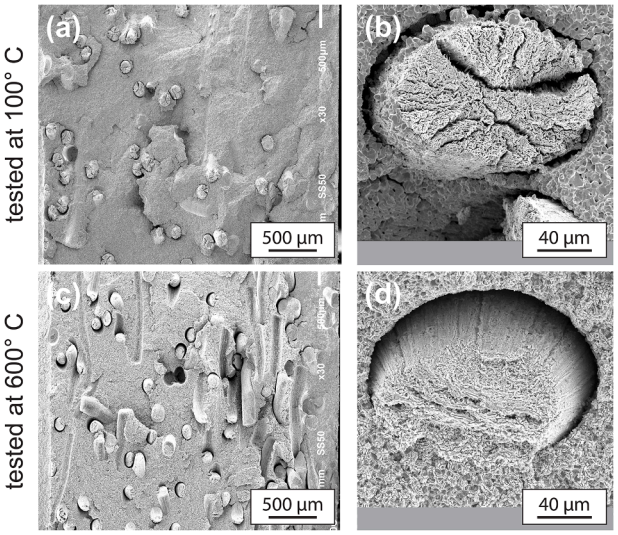

Fig. 5. Fracture surface of S-W_f/W in non-irradiated condition tested at 100 °C (a,b) and 580 °C (c,d). On the left overview pictures are shown . The artificial notch is on the left hand side of the picture. On the right a representative fibre is shown in larger magnification.

of IGP-W above DBTT. As observed before [8] the toughening effect is also smaller than for long-fibre reinforced material both before and after irradiation (compare Figs. 4 and 8). A reason why S-W_f/W does not perform as well as the long fibre material is that it has less fibres in loading direction and thus, ductile deformation is restricted to individual fibres [10]. In addition the fibres already show some degradation due to the powder metallurgical production process either due to the high sintering temperature of 1900 °C or the use of a graphite crucible. Doing this without a protective layer leads to an embrittlement of the W fibres, probably caused by an uptake of carbon into the material [20,21]. This behaviour is consistent with other studies where S-W_f/W shows low/no toughness at RT [21]. An attenuation of this embrittlement effect at elevated testing temperature could explain the observed increase in toughness. The different behaviour in the irradiated state could either be caused by a change in the interaction of the fibre and matrix or by a change in the fracture behaviour of the fibre, as the behaviour of the matrix does not change. We attribute this change to the effect of carbon on the fibre behaviour. Samples were held at elevated temperature for a long time during irradiation which facilitates the distribution of carbon from the matrix towards the fibres (C diffusion is temperature dependent [66]). This should be more pronounced for the higher irradiation temperature and thus explains the later onset of toughening for samples irradiated at 1000 °C. This would also explain why fibre ductility is affected in the short fibre material but not significantly altered for the long fibre material. Measurements of the carbon content within the fibres should be performed to validate this theory.

Only *L*-W_f/W shows toughness (defined by an increase in the fracture energy), observed as stable crack propagation at RT in the non-irradiated case. The long fibre samples show a higher toughness than S-W_f/W for all testing temperatures and than IGP-W up to its DBTT. Toughness is highest at 100 °C. Irradiation leads to a reduction of toughness, which is more pronounced at lower irradiation temperatures, but does not lead to embrittlement. In all cases, toughness initially decreases with increasing test temperature. In the irradiated case, it finally reaches a plateau, while in the non-irradiated case it rises again after 500 °C.

This behaviour corresponds to the force-displacement curves, which exhibit the characteristic shape of ductile materials for all test cases, both before and after irradiation (see Fig. 8). The shape of the curves can be related to the toughening mechanisms being active in L-W_f/W. Shape and fracture surfaces clearly point to ductile fibre bridging as dominating mechanism. During bending, there is a direct correlation between displacement and crack opening, and therefore also with the strain in the fibres, as these bridge the crack. Maximum in load is usually associated with a massive failure of the bridging fibres and can therefore be related to fibre strength [16]. Both directly influence the effectiveness of ductile fibre bridging [67]. The maximum load decreases with rising temperature (see Fig. 8). This corresponds well with the degradation of strength of tungsten fibres with rising temperature [19] and can explain the reduction in toughness of the samples observed for rising test temperatures. The lower fracture energy for lower irradiation temperature corresponds to lower maximum load in this case. However, more tests would be needed to confirm this behaviour. There has been only one sample per condition, and the difference is less then the error bar for non-irradiated samples, where more samples were tested.

For all irradiated samples (and non-irradiated samples at RT), the maximum load occurs at a lower displacement compared to the non-irradiated state at elevated temperature, which also explains the overall lower toughness. The change at elevated temperature for non-irradiated material could be explained by an increased ductility of the fibres (larger reduction in area at 100 °C compared to RT) which could have compensated for the reduction in strength. This is not a good explanation for the reduction in the irradiated case as fibre ductility, as defined by fibre diameter reduction, is not reduced (compared to the non-irradiated state). It is possible that there are other relationships between fibre strain and ductility and/or crack opening and fibre strain in the irradiated case. For example, it is reported that the constraint on the fibre, i.e. the interaction/bonding to the matrix has strong influence on the contribution by ductile deformation [67,68]. To confirm this, irradiation studies on the individual systems should be performed i.e. on the fibre-matrix-interface system for the role of the constraint or the individual fibre/wire for the effect on fracture strain. Neutron irradiation on individual fibres has been performed or is ongoing and evaluation by means of mechanical tests and microstructural analysis are planned. In addition studies by transmission electron microscopy (TEM) on ion irradiated W fibres with a thinner diameter are ongoing. Furthermore, TEM analysis has started for the samples presented in this study to give both insight in the damage caused by irradiation as well as the extent of transmutation.

The fracture behaviour of the matrix is cleavage for all test conditions, in contrast to Charpy impact tests on similar material, where a transition to ductile matrix failure was observed at 1000 °C [49]. This difference also applies to non-irradiated material and is therefore not caused by irradiation, but rather a consequence of the test conditions.

4.3. Conservation of ductility in W fibre

Similar to the non-irradiated case all W fibres in L-W_f/W show ductile failure with significant necking after irradiation (see Table 2). The necking diameter is very similar to the non-irradiated case up to a testing temperature of 500 °C and slightly larger for a testing temperature of 590 °C ± 10 °C. Only fibres irradiated at 600 °C and tested 100 °C show a significantly larger necking compared to the other conditions. Fig. 11 shows the reduced diameter as a function of the test temperature for the different cases and for an individual W fibre. Trend lines have been added as a visual guide. While a linear decrease can be observed in the non-irradiated case, the irradiated case levels off at higher test temperatures. This even seems to lead to a decrease in diameter reduction at higher test temperatures. However, tests above 590 °C ± 10 °C would be necessary for clarification, as the values are very close to each other in view of the error bars. Whether this change in behaviour is caused by a change in the behaviour of the individual fibre or by its interaction within the composite needs to be clarified.

During Charpy tests on non-irradiated, similar material with the same geometry [49] slightly less necking was observed at RT tests (118 µm ± 2 µm) and a slightly larger value for tests at 600 °C (69 µm ± 1 µm). This variation is in the same range as all differences observed after irradiation and therefore probably represents the natural spread.

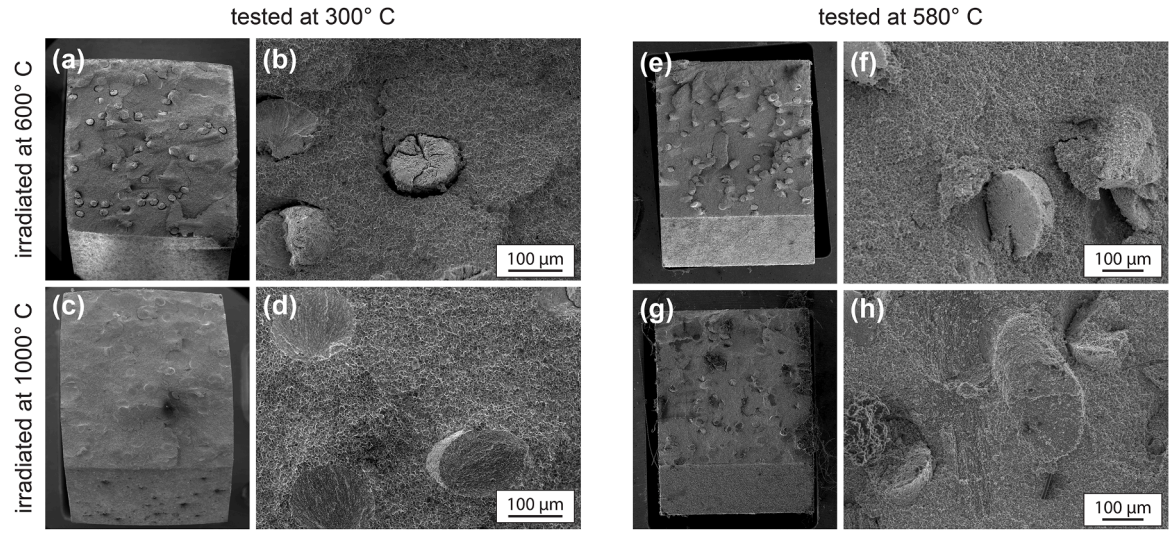

Fig. 6. Fracture surface of S-W_f/W samples which were irradiated at 600 °C (a,b,e,f) and 1000 °C (c,d,g,h) and tested at 300 °C and at 580 °C. In each case, overview pictures are shown on the left side (sample size 3 mm x 4 mm). The artificial notch is on the bottom side of the picture. On the right a representative region is shown in larger magnification.

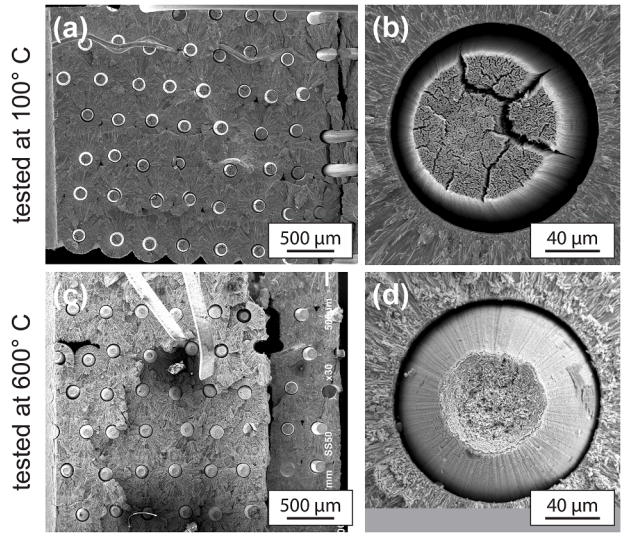

Fig. 7. Fracture surface of L-W_f/W in non-irradiated condition tested at 100 °C (a,b) and 600 °C (c,d). On the left an overview picture is shown . The artificial notch is on the left hand side of the picture. On the right a representative fibre is shown in larger magnification.

Although the different testing speed might play a role, this shows that the effect of irradiation on the ductile deformation of the W fibres might be low in our study. In the charpy tests the DBTT of the fibres was reported to be between −100 and −50 °C. The results in this study confirm that the DBTT is below RT before irradiation and below 100 °C after irradiation. However, as already pointed out in [25] a shift in DBTT by irradiation to a value below testing temperature would not have been detected in our studies.

In tungsten fibre-reinforced copper composites (W_f/Cu) ductile deformation was less pronounced for W fibres after irradiation (to similar damage level in W) showing both ductile and brittle fracture [69]. For a testing temperature of 150 °C necking was, for an irradiation temperature of 150 °C, in a similar range as in our study and was less pronounced for an irradiation temperature of 450 °C. To understand this, one needs to look at the differences in fibre-matrix interaction in the two composite systems. In W_f/Cu W fibres are used for strengthening rather than for toughening. This means that debonding is not desired and the matrix-fibre interface should be as strong as possible [8]. This, combined with the fact that fracture strain is much higher in the CuCrZr matrix [70], prevents non-constraint deformation and thus hinders necking. If the CuCrZr matrix is embrittled as reported for low irradiation temperatures, necking should be more pronounced compared to higher irradiation temperature where the matrix stays more ductile (see Fabritsiev and Pokrovsky [71] for irradiation effect on CuCrZr). As mentioned above, tests on the individual fibre/wire would allow for separation of the effects of constraint and irradiation on ductility. In contrast, ductility and its conservation during irradiation is better utilized in W_f/W as it relies on a brittle matrix. This is in line with findings by Zinovev et al. [72], who showed that individual tungsten foils are much more resistant to radiation embrittlement than when they are part of a composite.

Necking diameter in tensile tests of the individual fibre in the non-irradiated state were determined to be slightly larger by Riesch et al. [73] in RT tests. However, in studies of Terentyev et al. [19] they were slightly smaller at RT as well as at elevated temperature. Beside this spread, probably caused by different testing procedures, a reasonable explanation of the lower values in our studies is the constraint on the fibres provided by the composite structure.

The necking behaviour of W fibres with a diameter of 16 µm thinned to 5 µm was independent of damage by ion irradiation up to 10 dpa in RT tests [25,26]. This behaviour was attributed to defect annihilation at the grain boundaries in this ultra fine grained material and/or the special deformation mechanism below a diameter of 1 mm. W fibres with a diameter of 150 µm, used in the L-W_f/W composites, exhibits a similar deformation behaviour [73] and a fine micro structure [74]. Because of this, the same effects could explain the low influence of irradiation observed in our study. Transmutation typically seen as an important source for hardening/embrittlement seems to have no influence on the W fibre ductility for our experimental conditions. The TEM studies will help to understand the role of transmutation products. Neutron irradiation on fibres with a diameter of 150 µm is ongoing and will enable a better understanding of the role of transmutation. The results will also show whether, as with thin fibres, the irradiation has no effect on the mechanical behaviour. If this is the case, the observed changes in the necking behaviour after irradiation (compare Fig. 11) are likely caused by a change in the fibre-matrix interaction.

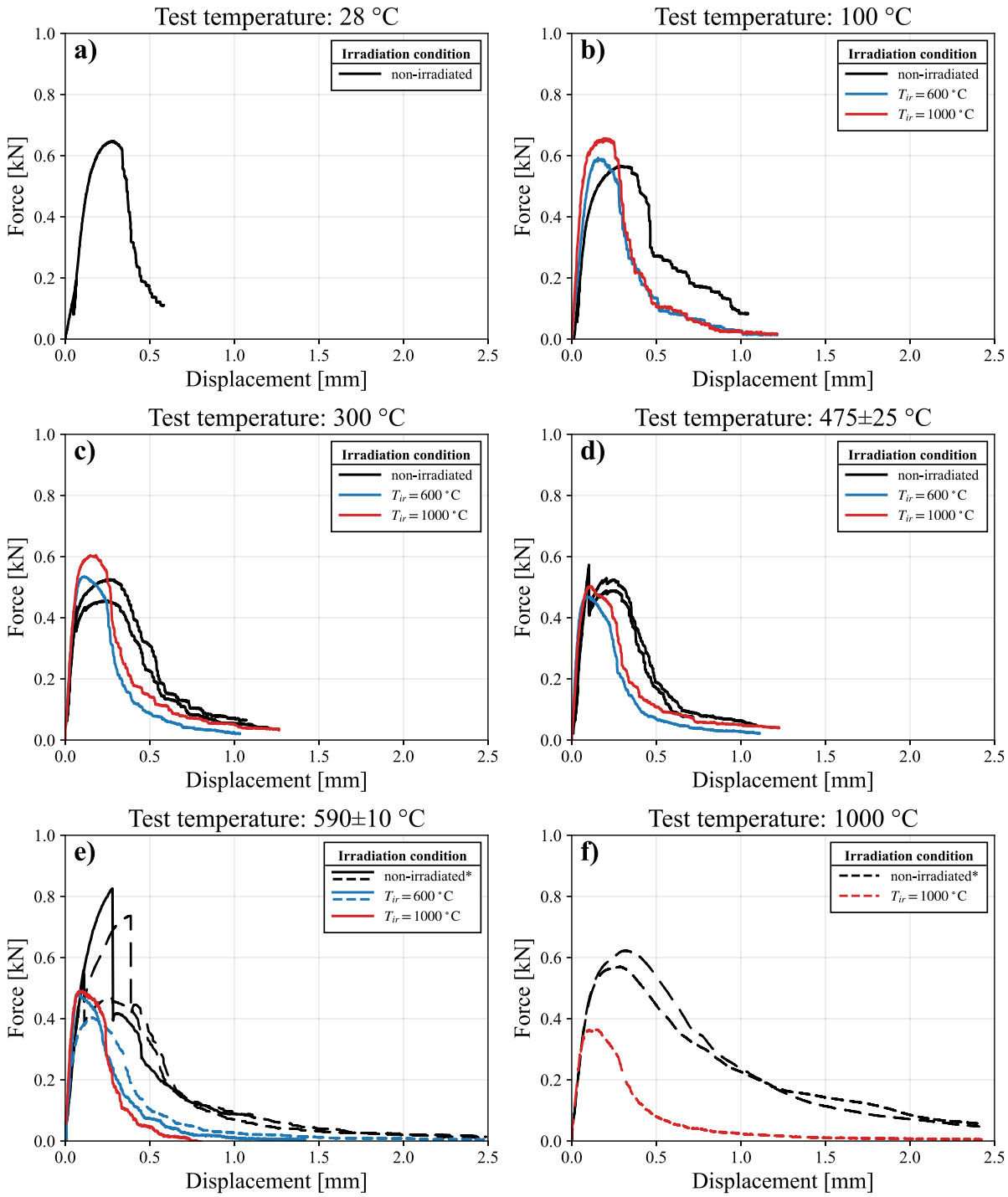

Fig. 8. Force-displacement curves of L-W_f/W before and after irradiation for different test temperatures. Black lines show non-irradiated material. Blue lines represents samples irradiated at 600 °C, red lines samples irradiated at 1000 °C. The span was 18 mm for tests up to 475 °C ± 25 °C (solid lines) and 25 mm for tests at 1000 °C (dashed lines). For tests at 590 °C ± 10 °C both spans were used. Non-irradiated samples tested with the larger span featured a smaller notch depth of 0.6 mm (indicated by (*)). (For interpretation of the references to colour in this figure legend, the reader is referred to the web version of this article.)

4.4. Irradiation effects on tungsten fibre-reinforced composites

After neutron irradiation L-W_f/W shows toughness down to the lowest testing temperature with only minor degradation compared to the non-irradiated state. This is a clear proof that extrinsic toughening is also effective after neutron irradiation. Fibre-Matrix debonding occurred during fracture and ductile fibre bridging was clearly identified to be the main toughening mechanism even after irradiation,with only small changes in ductile fibre deformation. This conservation is very beneficial as ductile fibre bridging is the most effective toughening mechanism in W_f/W. Nevertheless, the changes observed after irradiation, even if small, can probably be correlated to an effect on the fibre-matrix interface or the fibre properties. Influence of the heat treatment during irradiation is expected to be low due to the temperature stability of the

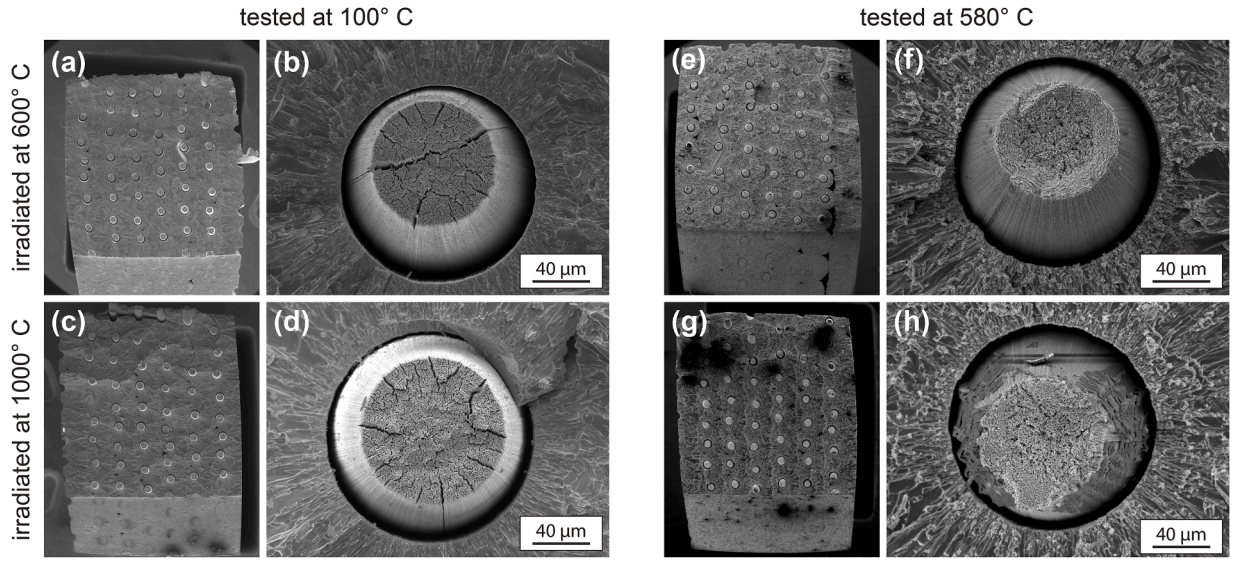

Fig. 9. Fracture surface of L-W_f/W samples which were irradiated at 600 °C (a,b,e,f) and 1000 °C (c,d,g,h) and tested at 100 °C and at 580 °C. In each case, overview pictures are shown on the left side (sample size 3 mm x 4 mm). The artificial notch is on the bottom side of the picture. On the right a representative fibre is shown in larger magnification for each test regime. The surface structures on the fibre seen in figure (h) is probably caused by oxidation and was also observed for fibres that were irradiated at 600 °C and tested at the same temperature.

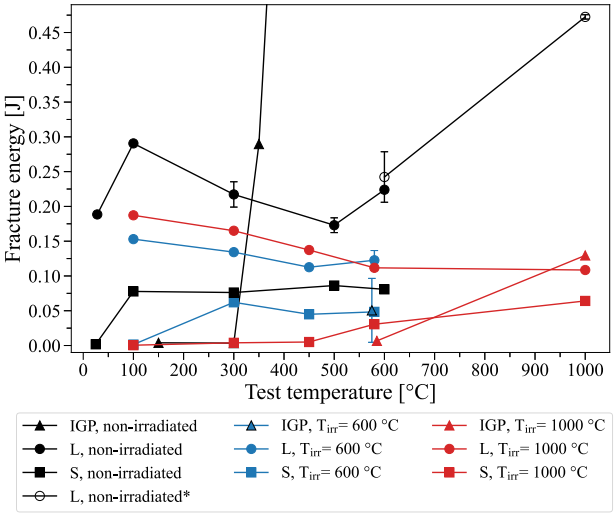

Fig. 10. Overview of fracture energies calculated as the integral of force over displacement. Results for IGP-W are shown as triangles, for S-W_f/W as squares and for L-W_f/W as circles. In the case of L-W_f/W open circles show data for samples featuring a smaller notch depth (indicated by (*)). Data points are shown in black for non-irradiated material, in blue for material irradiated at 600 °C and in red for material irradiated at 1000 °C. Typically only one sample per condition has been tested. If there are more samples, the mean and the standard deviation are given. (For interpretation of the references to colour in this figure legend, the reader is referred to the web version of this article.)

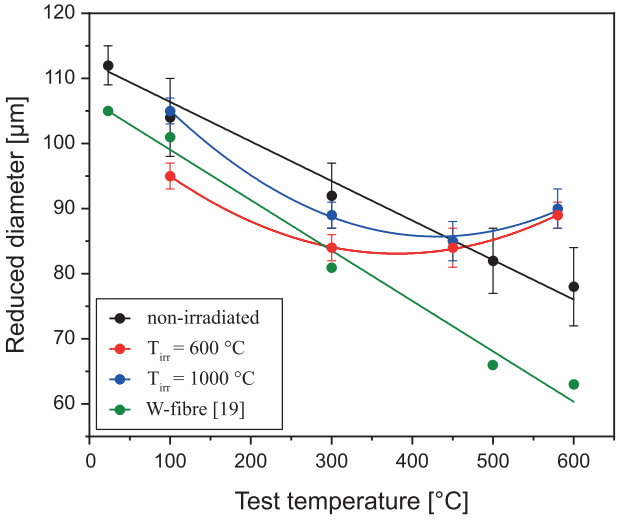

Fig. 11. Reduced diameter after fracture for L-W_f/W as a function of the test temperature according to Table 2. Data points are shown in black for non-irradiated material, in blue for material irradiated at 600 °C and in red for material irradiated at 1000 °C. In green data for the individual W fibre is given as determined in [19]. As a visual guide, trend lines are added (linear for non-irradiated and polynomial for irradiated material). (For interpretation of the references to colour in this figure legend, the reader is referred to the web version of this article.)

W wire used as fibre (see e.g. Nikolić et al. [18], Ciucani et al. [75] for more details). For a final clarification, test on the individual fibre or composite model systems would be helpful.

In L-W_f/W, the toughness and its resistance to irradiation induced degradation were significantly better than those of S-W_f/W, due to a better utilization of ductile fibre-bridging behaviour. It was shown that S-W_f/W can be produced while maintaining fibre ductility [12]. However, due to the better utilization of the fibre properties long fibre-reinforced material should be preferred. Recently, long fibre material utilizing a powder metallurgical production route was successfully qualified [76]. As long-fibre composites feature in general non isotropic behaviour fibres should be aligned in the direction of maximum stress.

Although the toughness of L-W_f/W is lower compared to IGP W above its DBTT, the low temperature toughness and the stability after irradiation provides room for design freedom. Predictable properties enable components to be designed in accordance with these properties. When looking at the proposed design of a high heat flux component there will always be a region where the temperature will be below the DBTT and the material therefore will exhibit brittle failure. This will even be more pronounced in the irradiated state. This temperature was found to be up to 1000 °C for IGP W after irradiation. The low DBTT of

L-W_f/W both before and after irradiation allows this region, which is considered critical in the design of these components [6], to be avoided or at least minimized.

The structure and composition of the composite materials used in this study were chosen to investigate the effect of irradiation on extrinsic toughening but were far from being optimised. Composites need to be designed according to their application especially non isotropic material as L-W_f/W [23]. Measures for improvement may include the following, among other things: a reduction of porosity, an increase of fibre volume fraction or the utilization of stronger fibres.

5. Conclusions

W_f/W was identified as a promising candidate for the high-heat flux region of a future fusion reactor as it shows increased toughness due to extrinsic toughening mechanisms. However, the effect of neutron irradiation on these mechanisms has been an open question. In this study short and long fibre-reinforced W_f/W as well as IGP W as a reference material have been irradiated up to 0.7-0.8 dpa at 600 °C and 1000 °C. 3-point bending tests were used to evaluate the effect of neutron irradiation on the toughness. For IGP W the DBTT increased from 300 °C to at least 600 °C (irradiation temperature 600 °C) and to at least 1000 °C (irradiation temperature 1000 °C). For S-W_f/W it increases from 100 °C to 300 °C (irradiation temperature 600 °C) and 600 °C (irradiation temperature 1000 °C). L-W_f/W shows toughness at RT in the non-irradiated state and down to the lowest testing temperature of 100 °C after irradiation. Above the DBTT, the fracture energies, which serve as a measure for toughness, are higher in L-W_f/W than in S-W_f/W, both in the non-irradiated and irradiated states. For L-W_f/W fracture energies decrease slightly due to irradiation, but the decrease is very similar for both irradiation temperatures. At a test temperature of 300 °C, non-irradiated L-W_f/W exhibits a fracture energy of $0.22\,J \pm 0.02\,J$, compared to 0.13 J and 0.17 J after irradiation.

The main conclusions are

- Extrinsic toughening remained active in W_f/W after neutron irradiation with the ductile fibre bridging being the dominating mechanism.
- Neutron irradiation up to 0.8 dpa had only a minor influence on the fracture behaviour of L-W_f/W
- W fibres in L-W_f/W stayed ductile and showed only slight deterioration due to neutron irradiation.

This behaviour provides design freedom and now needs to be incorporated into the design of new components as proposed in [23]. Further tests should be performed to understand the resistance of the W fibre ductility against irradiation embrittlement e.g. utilizing neutron irradiation experiments on individual W fibres or using the new experimental setup GIRAFFE [77] which allows mechanical testing of thin W fibres during in-situ irradiation by high energetic ions.

CRediT authorship contribution statement

J. Riesch: Writing – original draft, Visualization, Validation, Supervision, Methodology, Formal analysis, Conceptualization; **A. Zinovev:** Writing – review & editing, Methodology, Investigation, Formal analysis; **E. Gaganidze:** Writing – review & editing, Supervision, Investigation, Formal analysis; **H. Ries:** Methodology, Investigation; **H. Gietl:** Writing – review & editing, Resources; **Y. Mao:** Writing – review & editing, Resources; **J. W. Coenen:** Writing – review & editing, Project administration; **T. Höschen:** Writing – review & editing, Investigation, Formal analysis, Conceptualization; **D. Terentyev:** Writing – review & editing, Investigation, Funding acquisition, Formal analysis, Data curation, Conceptualization; **R. Neu:** Writing – review & editing, Funding acquisition.

Data availability

Data will be made available on request.

Declaration of competing interest

The authors declare that they have no known competing financial interests or personal relationships that could have appeared to influence the work reported in this paper.

Acknowledgment

We would like to thank Jürgen Almanstötter and Maximillian Weik for their support in visualizing the force-displacement curves. This work has been carried out within the framework of the EUROfusion Consortium, funded by the European Union via the Euratom Research and Training Programme (Grant Agreement Nos. 633053 and 101052200 - EUROfusion). Views and opinions expressed are however those of the author(s) only and do not necessarily reflect those of the European Union or the European Commission. Neither the European Union nor the European Commission can be held responsible for them.

Appendix A. Chemical analysis

In Table A.1, the chemical composition of W wire and W produced by CVD is given. The wire was produced with a similar fabrication process from the same supplier as the wire used in this study (both for S- and L-W_f/W). The CVD material has been produced in a similar process on the same device as the L-W_f/W plates. O and C were determined using combustion analysis. The other elements are determined by a combination of inductively coupled plasma mass spectrometry (HR ICP-MS) and inductively coupled plasma optical emission spectrometry (ICP-OES).

Table A.1
Chemical composition of W wire and W produced by CVD. The wire was produced with a similar fabrication process from the same supplier as the wire used in this study (both for S- and L-W_f/W). The CVD material has been produced in a similar process on the same device as the L-W_f/W plates.

Element	*W wire* $\mu g \cdot g^{-1}$	*CVD W* $\mu g \cdot g^{-1}$
Al	9.1 ± 0.1	< 0.1
Ca	< 0.3	< 0.3
Co	< 0.1	< 0.1
Cr	2.6 ± 0.1	< 0.1
Cu	< 0.1	< 0.1
Fe	7.0	< 0.1
K	72 ± 2	0.3 ± 0.1
Mo	10.2 ± 0.3	< 0.1
Na	0.7 ± 0.3	< 0.1
Ni	< 0.3	< 0.3
Os	< 2	< 2
Re	no measurement possible	
Si	< 3	< 3
Ta	< 2	0.1 ± 0.1
Ti	0.3 ± 0.1	0.1 ± 0.1
V	8.1	< 0.1
O*	88.5 ± 1.8	139.0 ± 18.4
C*	37.5 ± 1.8	22.3 ± 2.0

* Based on measurement of 2–3 samples, error given as standard deviation of the mean

Appendix B. Cutting scheme of W_f/W samples

In Fig. B.1 the cutting scheme of the plates and disks is shown. The samples were orientated in a way that the fibre axis are along the long side for the L-W_f/W material.

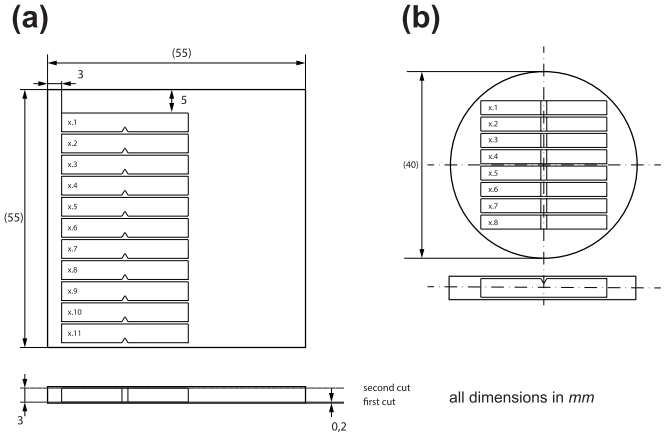

Fig. B.1. Cutting scheme of KLST type samples for (a) the L-W_f/W material and (b) for the S-W_f/W material. All dimensions are given in mm.

Appendix C. Evaluation force-displacement curves

A robust estimate of the pre-peak elastic response is obtained by fitting a linear model $f \approx a(d - D_0) = a\,d + b$ to the low-force portion of the paired displacement-force datasets (d_i, f_i). After removing invalid data points and optionally correcting a constant force baseline, contiguous sliding windows of varying length are scanned over the ordered data. Each window that satisfies toe- and span-filters (to ensure the window starts sufficiently

far from zero force and guarantee that the force variation inside the window is large enough to determine a slope) is evaluated with a mean centred ordinary least-squares (OLS) estimator constrained to $a > 0$. Within each admissible window $\mathcal{I}$ we compute a mean-centred OLS line

$$\hat{a}(\mathcal{I}) = \frac{\sum_{i\in\mathcal{I}}(d_i - \bar{d}_\mathcal{I})(f_i - \bar{f}_\mathcal{I})}{\sum_{i\in\mathcal{I}}(d_i - \bar{d}_\mathcal{I})^2}, \qquad \hat{b}(\mathcal{I}) = \bar{f}_\mathcal{I} - \hat{a}(\mathcal{I})\,\bar{d}_\mathcal{I}, \tag{C.1}$$

and evaluate its goodness of fit by the coefficient of determination

$$R^2(\mathcal{I}) = 1 - \frac{\sum_{i\in\mathcal{I}}\left(f_i - \hat{a}(\mathcal{I})d_i - \hat{b}(\mathcal{I})\right)^2}{\sum_{i\in\mathcal{I}}(f_i - \bar{f}_\mathcal{I})^2}, \tag{C.2}$$

as well as the force span

$$\Delta f(\mathcal{I}) = \max_{i\in\mathcal{I}} f_i - \min_{i\in\mathcal{I}} f_i. \tag{C.3}$$

The window maximizing the lexicographic score $(\hat{a}, R^2, \Delta f)$ above a descending set of R^2 thresholds is selected, and its horizontal shift is recovered from $\widehat{D}_0 = -\hat{b}/\hat{a}$.Â This procedure yields a physically meaningful elastic slope and offset even in the presence of noise or limited data. All experimental datasets are shifted by $\widehat{D}_0$, no further points representing the elastic line were inserted.

Appendix D. Overview of results of fracture mechanical tests

In Table D.1, an overview of results of the fracture mechanical tests is given. The first column shows the test temperature. In the other columns the main behaviour of the samples is stated .

Table D.1
Overview of results of fracture mechanical tests. The first column shows the test temperature in °C. In the other columns the main behaviour of the samples is given: x for brittle behaviour, o for tough behaviour / b for brittle fibre failure, d for ductile fibre failure, - for not applicable, brackets for transitions or non conclusive behaviour.

	IGP W			*S-W_f/W*			*L-W_f/W*		
	Non-irradiated	*Irradiated at 600 °C*	*Irradiated at 1000 °C*	*Non-irradiated*	*Irradiated at 600 °C*	*Irradiated at 1000 °C*	*Non-irradiated*	*Irradiated at 600 °C*	*Irradiated at 1000 °C*
RT				x/b			o/d		
100				o/d	x/b	x/b	o/d	o/d	o/d
150	x/-								
300	x/-			o/d	o/d	x/b	o/d	o/d	o/d
350	(o)/-								
475 ± 25	o/-	x/-	x/-	o/d	o/d	x/(d)	o/d	o/d	o/d
590 ± 10	o/-	(o)/-	x/-	o/d	o/d	(o)/(d)	o/d	o/d	o/d
1000			o/-			o/-			o/-

Appendix E. Fracture energies

In Table E.1, the fracture energies calculated as the integral of force over displacement as given in Figs. 2,4 and 8 are shown. These values are illustrated as a digram in Fig. 10.

Table E.1
Overview of fracture energies calculated as the integral of force over displacement. The first column shows the test temperature in °C. In the case of L-W_f/W data for samples featuring a smaller notch depth is indicated by (*). Typically only one sample per condition has been tested. In this case only the value of the integral is shown. If there are more samples, the mean and the standard deviation are given.

	IGP W			*S-W_f/W*			*L-W_f/W*		
	Non-irradiated	*Irradiated at 600 °C*	*Irradiated at 1000 °C*	*Non-irradiated*	*Irradiated at 600 °C*	*Irradiated at 1000 °C*	*Non-irradiated*	*Irradiated at 600 °C*	*Irradiated at 1000 °C*
RT				0.002 J			0.19 J		
100				0.08 J	0.001 J	0.0004 J	0.29 J	0.15 J	0.19 J
150	0.004 J								
300	0.003 J			0.08 J	0.06 J	0.004 J	0.22 J ± 0.02 J	0.13 J	0.17 J
350	0.29 J								
450	1.57 J				0.04 J	0.005 J		0.11 J	0.14 J
500	2.33 J			0.09 J			0.17 J ± 0.01 J		
590 ± 10	2.78 J	0.05 J ± 0.05 J	0.01 J	0.08 J	0.05 J	0.03 J	0.22 J / (0.24 J ± 0.04 J)*	0.12 J ± 0.01 J	0.11 J
1000			0.13 J			0.06 J	(0.47 J)*		0.11 J

References

[1] J.W. Coenen, S. Antusch, M. Aumann, W. Biel, J. Du, J. Engels, S. Heuer, A. Houben, T. Hoeschen, B. Jasper, F. Koch, J. Linke, A. Litnovsky, Y. Mao, R. Neu, G. Pintsuk, J. Riesch, M. Rasinski, J. Reiser, M. Rieth, A. Terra, B. Unterberg, T. Weber, T. Wegener, J.-H. You, C. Linsmeier, et al., Materials for DEMO and reactor applications—boundary conditions and new concepts, Phys. Scr. T167 (2016) 014002. https://doi.org/10.1088/0031-8949/2016/T167/014002

[2] G. Pintsuk, A. Hasegawa, Tungsten as a plasma-facing material, in: Comprehensive Nuclear Materials, Elsevier, 2020, pp. 19–53. https://doi.org/10.1016/B978-0-12-803581-8.11696-0

[3] J.H. You, G. Mazzone, E. Visca, H. Greuner, M. Fursdon, Y. Addab, C. Bachmann, T. Barrett, U. Bonavolontà, B. Böswirth, F.M. Castrovinci, C. Carelli, D. Coccorese, R. Coppola, F. Crescenzi, G. Di Gironimo, P.A. Di Maio, G. Di Mambro, F. Domptail, Dongiovanni, G. Dose, D. Flammini, L. Forest, P. Frosi, F. Gallay, B.E. Ghidersa, C. Harrington, K. Hunger, V. Imbriani, M. Li, A. Lukenskas, A. Maffucci, N. Mantel, Marzullo, T. Minniti, A.V. Müller, S. Noce, M.T. Porfiri, A. Quartararo, M. Richou, S. Roccella, D. Terentyev, A. Tincani, E. Vallone, S. Ventre, R. Villari, F. Villone, C. Vorpahl, K. Zhang, et al., Divertor of the European DEMO: engineering and technologies for power exhaust, Fusion Eng. Des. 175 (2022) 113010. https://doi.org/10.1016/j.fusengdes.2022.113010

[4] S. Nogami, A. Hasegawa, M. Fukuda, M. Rieth, J. Reiser, G. Pintsuk, et al., Mechanical properties of tungsten: recent research on modified tungsten materials in Japan, J. Nucl. Mater. 543 (2021) 152506. https://doi.org/10.1016/j.jnucmat.2020.152506

[5] J.W. Coenen, Fusion materials development at forschungszentrum Jülich, Adv. Eng. Mater. 22 (6) (2020) 1901376. https://doi.org/10.1002/adem.201901376

[6] G. Pintsuk, E. Diegele, S.L. Dudarev, M. Gorley, J. Henry, J. Reiser, M. Rieth, et al., European materials development: results and perspective, Fusion Eng. Des. 146 (2019) 1300–1307. https://doi.org/10.1016/j.fusengdes.2019.02.063

[7] C. Linsmeier, M. Rieth, J. Aktaa, T. Chikada, A. Hoffmann, J. Hoffmann, A. Houben, H. Kurishita, X. Jin, M. Li, A. Litnovsky, S. Matsuo, A. von Mueller, V. Nikolic, T. Palacios, R. Pippan, D. Qu, J. Reiser, J. Riesch, T. Shikama, R. Stieglitz, T. Weber, S. Wurster, J.-H. You, Z. Zhou, et al., Development of advanced high heat flux and plasma-facing materials, Nucl. Fusion 57 (9) (2017). https://doi.org/10.1088/1741-4326/aa6f71

[8] J. Riesch, M. Fuhr, J. Almanstötter, et al., Tungsten wire—from lamp filaments to reinforcement fibers for composites in fusion reactors, Adv. Eng. Mater. (2024). https://doi.org/10.1002/adem.202400951

[9] D.A.H. Wartacz, T. Höschen, J. Riesch, K. Pantleon, W. Pantleon, et al., Thermal stability of multi-fiber tungsten fiber-reinforced tungsten composites and their mechanical integrity after high temperature annealing, Fusion Eng. Des. 222 (2026) 115438. https://doi.org/10.1016/j.fusengdes.2025.115438

[10] Y. Mao, J.W. Coenen, J. Riesch, S. Sistla, J. Almanstötter, B. Jasper, A. Terra, T. Höschen, H. Gietl, C. Linsmeier, C. Broeckmann, et al., Influence of the interface strength on the mechanical properties of discontinuous tungsten fiber-reinforced tungsten composites produced by field assisted sintering technology, Composites Part A Appl. Sci. Manuf. 107 (2018) 342–353. https://doi.org/10.1016/j.compositesa.2018.01.022

[11] J. Riesch, Y. Han, J. Almanstötter, J.W. Coenen, T. Höschen, B. Jasper, P. Zhao, C. Linsmeier, R. Neu, et al., Development of tungsten fibre-reinforced tungsten composites towards their use in DEMO—potassium doped tungsten wire, Phys. Scr. T167 (2016) 014006. https://doi.org/10.1088/0031-8949/T167/1/014006

[12] Y. Mao, J.W. Coenen, J. Riesch, S. Sistla, J. Almanstötter, J. Reiser, A. Terra, C. Chen, Y. Wu, L. Raumann, T. Höschen, H. Gietl, R. Neu, C. Linsmeier, C. Broeckmann, et al., Fracture behavior of random distributed short tungsten fiber-reinforced tungsten composites, Nucl. Fusion 59 (8) (2019) 086034. https://doi.org/10.1088/1741-4326/ab25b0

[13] H. Gietl, S. Olbrich, J. Riesch, G. Holzner, T. Höschen, J.W. Coenen, R. Neu, et al., Estimation of the fracture toughness of tungsten fibre-reinforced tungsten composites, Eng. Fract. Mech. 232 (2020) 107011. https://doi.org/10.1016/j.engfracmech.2020.107011

[14] A.G. Evans, Perspective on the development of high–Toughness ceramics, J. Am. Ceram. Soc. 73 (2) (1990) 187–206. https://doi.org/10.1111/j.1151-2916.1990.tb06493.x

[15] J. Riesch, J.-Y. Buffiere, T. Höschen, M. Scheel, C. Linsmeier, J.H. You, et al., Crack bridging in as-fabricated and embrittled tungsten single fibre-reinforced tungsten composites shown by a novel in-situ high energy synchrotron tomography bending test, Nucl. Mater. Energy 15 (2018) 1–12. https://doi.org/10.1016/j.nme.2018.03.007

[16] H. Gietl, J. Riesch, J.W. Coenen, T. Höschen, C. Linsmeier, R. Neu, et al., Tensile deformation behavior of tungsten fibre-reinforced tungsten composite specimens in as-fabricated state, Fusion Eng. Des. 124 (2017) 396–400. https://doi.org/10.1016/j.fusengdes.2017.02.054

[17] D. Schwalenberg, J.W. Coenen, J. Riesch, T. Hoeschen, Y. Mao, A. Lau, H. Gietl, L. Raumann, P. Huber, C. Linsmeier, R. Neu, et al., Large-scale tungsten fibre-reinforced Tungsten and its mechanical properties, J. Nucl. Eng. 3 (4) (2022) 306–320. https://doi.org/10.3390/jne3040018

[18] V. Nikolić, J. Riesch, R. Pippan, et al., The effect of heat treatments on pure and potassium doped drawn tungsten wires: Part I - Microstructural characterization, Mater. Sci. Eng. A 737 (2018) 422–433. http://www.sciencedirect.com/science/article/pii/S0921509318312243. https://doi.org/10.1016/j.msea.2018.09.027

[19] D. Terentyev, J. Riesch, S. Lebediev, A. Bakaeva, J.W. Coenen, et al., Mechanical properties of as-fabricated and 2300 °C annealed tungsten wire tested up to 600 °C, Int. J. Refract. Met. Hard Mater 66 (2017) 127–134. https://doi.org/10.1016/j.ijrmhm.2017.03.011

[20] A.V. Müller, M. Ilg, H. Gietl, T. Höschen, R. Neu, G. Pintsuk, J. Riesch, U. Siefken, J.H. You, et al., The effects of heat treatment at temperatures of 1100 °C to 1300 °C on the tensile properties of high-strength drawn tungsten fibres, Nucl. Mater. Energy 16 (2018) 163–167. https://doi.org/10.1016/j.nme.2018.06.003

[21] Y. Mao, C. Chen, J.W. Coenen, J. Riesch, S. Sistla, J. Almanstötter, A. Terra, Y. Wu, L. Raumann, T. Höschen, H. Gietl, R. Neu, C. Linsmeier, C. Broeckmann, et al., On the nature of carbon embrittlement of tungsten fibers during powder metallurgical processes, Fusion Eng. Des. 145 (2019) 18–22. https://doi.org/10.1016/j.fusengdes.2019.05.033

[22] D. Stork, P. Agostini, J.L. Boutard, D. Buckthorpe, E. Diegele, S.L. Dudarev, C. English, G. Federici, M.R. Gilbert, S. Gonzalez, A. Ibarra, C. Linsmeier, A. Li Puma, G. Marbach, P.F. Morris, L.W. Packer, B. Raj, M. Rieth, M.Q. Tran, D.J. Ward, S.J. Zinkle, et al., Developing structural, high-heat flux and plasma facing materials for a near-term DEMO fusion power plant: the EU assessment, J. Nucl. Mater. 455 (1–3) (2014) 277–291. https://doi.org/10.1016/j.jnucmat.2014.06.014

[23] J. Riesch, A. von Müller, Y. Mao, J.W. Coenen, B. Böswirth, S. Elgeti, M. Fuhr, H. Greuner, T. Höschen, K. Hunger, P. Junghanns, A. Lau, S. Roccella, L. Vanlitsenburgh, J.-H. You, C. Linsmeier, R. Neu, et al., Progress in the development of industrial scale tungsten fibre-reinforced composite materials, Nucl. Mater. Energy 38 (2024) 101591. https://doi.org/10.1016/j.nme.2024.101591

[24] Y. Katoh, T. Nozawa, C. Shih, K. Ozawa, T. Koyanagi, W. Porter, L.L. Snead, et al., High-dose neutron irradiation of hi-nicalon type s silicon carbide composites. Part 2: mechanical and physical properties, J. Nucl. Mater. 462 (2015) 450–457. https://doi.org/10.1016/j.jnucmat.2014.12.121

[25] J. Riesch, A. Feichtmayer, J.W. Coenen, B. Curzadd, H. Gietl, T. Höschen, A. Manhard, T. Schwarz-Selinger, R. Neu, et al., Irradiation effects in tungsten—From surface effects to bulk mechanical properties, Nucl. Mater. Energy 30 (2022) 101093. https://doi.org/10.1016/j.nme.2021.101093

[26] R. Lürbke, J. Riesch, A. Feichtmayer, B. Curzadd, T. Höschen, R. Neu, et al., Experimental investigation of the impact of irradiation damages on the mechanical properties of tungsten, Nucl. Mater. Energy 42 (2025) 101858. https://doi.org/10.1016/j.nme.2024.101858

[27] S.J. Zinkle, J.T. Busby, Structural materials for fission & fusion energy, Mater. Today 12 (11) (2009) 12–19. https://doi.org/10.1016/S1369-7021(09)70294-9

[28] G.S. Was, Fundamentals of Radiation Materials Science: Metals and Alloys, Springer New York, New York, NY and s.l., 2nd ed. 2017 edition, New York, NY and s.l., 2017. https://doi.org/10.1007/978-1-4939-3438-6

[29] E. Gaganidze, A. Chauhan, H.-C. Schneider, D. Terentyev, B. Rossaert, J. Aktaa, et al., Effect of irradiation temperature on the fracture-mechanical behaviour of tungsten irradiated to 1 dpa, J. Nucl. Mater. 556 (2021) 153200. https://doi.org/10.1016/j.jnucmat.2021.153200

[30] D. Terentyev, M. Rieth, G. Pintsuk, J. Riesch, A. von Müller, S. Antusch, K. Mergia, E. Gaganidze, H.-C. Schneider, M. Wirtz, S. Nogami, J. Coenen, J.H. You, A. Zinovev, W. van Renterghem, et al., Recent progress in the assessment of irradiation effects for in-vessel fusion materials: tungsten and copper alloys, Nucl. Fusion 62 (2) (2022) 026045. https://doi.org/10.1088/1741-4326/ac4062

[31] M.R. Gilbert, J.C. Sublet, Neutron-induced transmutation effects in W and W-alloys in a fusion environment, Nucl. Fusion 51 (4) (2011) 043005. https://doi.org/10.1088/0029-5515/51/4/043005

[32] P.D. Edmondson, A. London, A. Xu, D.E.J. Armstrong, S.G. Roberts, et al., Small-scale characterisation of irradiated nuclear materials: Part I – Microstructure, J. Nucl. Mater. 462 (2015) 369–373. https://doi.org/10.1016/j.jnucmat.2014.11.067

[33] D.E.J. Armstrong, C.D. Hardie, J.S.K.L. Gibson, A.J. Bushby, P.D. Edmondson, S.G. Roberts, et al., Small-scale characterisation of irradiated nuclear materials: Part II nanoindentation and micro-cantilever testing of ion irradiated nuclear materials, J. Nucl. Mater. 462 (2015) 374–381. https://doi.org/10.1016/j.jnucmat.2015.01.053

[34] A. Hasegawa, M. Fukuda, K. Yabuuchi, S. Nogami, Neutron irradiation effects on the microstructural development of tungsten and tungsten alloys, J. Nucl. Mater 471 (2016) 175–183. https://doi.org/10.1016/j.jnucmat.2015.10.047

[35] Y. Katoh, L.L. Snead, L.M. Garrison, X. Hu, T. Koyanagi, C.M. Parish, P.D. Edmondson, M. Fukuda, T. Hwang, T. Tanaka, A. Hasegawa, Response of unalloyed tungsten to mixed spectrum neutrons, J. Nucl. Mater.s 520 (2019) 193–207. https://doi.org/10.1016/j.jnucmat.2019.03.045

[36] G.S. Was, R.S. Averback, Radiation damage using ion beams, in: R. Konings (Ed.), Comprehensive Nuclear Materials, Elsevier Science, Burlington, 2011, pp. 195–221. https://doi.org/10.1016/B978-0-08-056033-5.00007-0

[37] G.S. Was, Challenges to the use of ion irradiation for emulating reactor irradiation, J. Mater. Res. 30 (9) (2015) 1158–1182. https://doi.org/10.1557/jmr.2015.73

[38] A.E. Committee, E521 – 16: Practice for Neutron Radiation Damage Simulation by Charged-Particle Irradiation. https://doi.org/10.1520/E0521-16

[39] S.M. G.D. Vicente, J.-L. Boutard, S.J. Zinkle, H. Tanigawa, Materials testing facilities and programmes for fission and ion implantation damage, Nucl. Fusion 57 (2017) 92011. https://doi.org/10.1088/1741-4326/aa6a67

[40] S. Das, Recent advances in characterising irradiation damage in tungsten for fusion power, SN Appl. Sci. 1 (12) (2019). https://doi.org/10.1007/s42452-019-1591-0

[41] N. Castin, D. Terentyev, A. Bakaev, A. Stankovskiy, G. Bonny, et al., On the equivalence of irradiation conditions on present and future facilities for fusion materials research and qualification: a computational study, J. Nucl. Mater. 562 (2022) 153589. https://doi.org/10.1016/j.jnucmat.2022.153589

[42] H. Gietl, M.J. Worrall, D.B. Chapman, J.M.E. Dromey, D. Frazer, S. Gonderman, J.V. Brookman, N.E. Woolstenhulme, et al., Neutron irradiation & thermomechanical experiment (NITE) - design, Fusion Eng. Des. 222 (2026) 115539. https://doi.org/10.1016/j.fusengdes.2025.115539

[43] S.J. Zinkle, A. Möslang, T. Muroga, H. Tanigawa, Multimodal options for materials research to advance the basis for fusion energy in the ITER era, Nucl. Fusion 53 (10) (2013) 104024. https://doi.org/10.1088/0029-5515/53/10/104024

[44] D. Terentyev, C. Yin, A. Dubinko, C.C. Chang, J.H. You, et al., Neutron irradiation hardening across ITER diverter tungsten armor, Int. J. Refract. Met. Hard Mater 95 (2021) 105437. https://doi.org/10.1016/j.ijrmhm.2020.105437

[45] E. Lucon, C. McCowan, R. Santoyo, J. Splett, et al., Standard reference materials (r) certification report for SRM 2216, 2218, 2219: KLST (miniaturized) charpy V-notch impact specimens. https://doi.org/10.6028/NIST.SP.260-180

[46] J. Riesch, M. Aumann, J.W. Coenen, H. Gietl, G. Holzner, T. Höschen, P. Huber, M. Li, C. Linsmeier, R. Neu, et al., Chemically deposited tungsten fibre-reinforced tungsten – The way to a mock-up for divertor applications, Nucl. Mater. Energy 9 (2016) 75–83. https://doi.org/10.1016/j.nme.2016.03.005

[47] H. Gietl, A.V. Müller, J.W. Coenen, M. Decius, D. Ewert, T. Höschen, P. Huber, M. Milwich, J. Riesch, R. Neu, et al., Textile preforms for tungsten fibre-reinforced composites, J. Compos. Mater. 52 (28) (2018) 3875–3884. https://doi.org/10.1177/0021998318771149

[48] Y. Mao, J.W. Coenen, J. Riesch, S. Sistla, J. Almanstötter, B. Jasper, A. Terra, T. Höschen, H. Gietl, M. Bram, J. Gonzalez-Julian, C. Linsmeier, C. Broeckmann, et al., Development and characterization of powder metallurgically produced discontinuous tungsten fiber reinforced tungsten composites, Phys. Scr. T170 (2017) 014005. https://doi.org/10.1088/0031-8949/2017/T170/014005

[49] H. Gietl, J. Riesch, T. Höschen, M. Rieth, J.W. Coenen, R. Neu, et al., Charpy impact tests of tungsten fiber–reinforced composite from −150 °C to 1000 °C, Mater. Lett. 311 (2022) 131526. https://doi.org/10.1016/j.matlet.2021.131526

[50] Y. Mao, J. Engels, A. Houben, M. Rasinski, J. Steffens, A. Terra, C. Linsmeier, J.W. Coenen, et al., The influence of annealing on yttrium oxide thin film deposited by reactive magnetron sputtering: process and microstructure, Nucl. Mater. Energy 10 (2017) 1–8. https://doi.org/10.1016/j.nme.2016.12.031

[51] M. Wirtz, J. Linke, T. Loewenhoff, G. Pintsuk, I. Uytdenhouwen, et al., Thermal shock tests to qualify different tungsten grades as plasma facing material, Phys. Scr. T167 (2016) 014015. https://doi.org/10.1088/0031-8949/T167/1/014015

[52] C. Yin, D. Terentyev, T. Pardoen, A. Bakaeva, R. Petrov, S. Antusch, M. Rieth, M. Vilémová, J. Matějíček, T. Zhang, et al., Tensile properties of baseline and advanced tungsten grades for fusion applications, Int. J. Refract. Met. Hard Mater. 75 (2018) 153–162. https://doi.org/10.1016/j.ijrmhm.2018.04.003

[53] E. Gaganidze, A. Chauhan, H.-C. Schneider, D. Terentyev, G. Borghmans, J. Aktaa, et al., Fracture-mechanical properties of neutron irradiated ITER specification tungsten, J. Nucl. Mater. 547 (2021) 152761. https://doi.org/10.1016/j.jnucmat.2020.152761

[54] A.E. Committee, E2248 – 18: Test Method for Impact Testing of Miniaturized Charpy V-Notch Specimens, . https://doi.org/10.1520/E2248-18

[55] D. Pelowitz, J. Durkee, J. Elson, M. Fensin, J. Hendricks, M. James, R. Johns, G. Mc Kinney, S. Mashnik, L. Waters, T. Wilcox, J. Verbeke, MCNPX 2.7.0 extensions, https://doi.org/10.2172/1058045

[56] P. Vajda, M. Biget, A. Lucasson, P. Lucasson, et al., On the problem of displacement threshold determination in irradiated metals: subthreshold effects and recovery spectrum, J. Phys. F Met. Phys. 7 (5) (1977) L123–L126. https://doi.org/10.1088/0305-4608/7/5/002

[57] F. Maury, M. Biget, P. Vajda, A. Lucasson, P. Lucasson, et al., Frenkel pair creation and stage I recovery in W crystals irradiated near threshold, Radiat. Eff. 38 (1–2) (1978) 53–65. https://doi.org/10.1080/00337577808233209

[58] Y. Iwamoto, S.-i. Meigo, S. Hashimoto, Estimation of reliable displacements-per-atom based on athermal-recombination-corrected model in radiation environments at nuclear fission, fusion, and accelerator facilities, J. Nucl. Mater. 538 (2020) 152261. https://doi.org/10.1016/j.jnucmat.2020.152261

[59] A.Y. Konobeyev, U. Fischer, Y.A. Korovin, S.P. Simakov, et al., Evaluation of effective threshold displacement energies and other data required for the calculation of advanced atomic displacement cross-sections, Nucl. Energy Technol. 3 (3) (2017) 169–175. https://doi.org/10.1016/j.nucet.2017.08.007

[60] K. Nordlund, S.J. Zinkle, A.E. Sand, F. Granberg, R.S. Averback, R. Stoller, T. Suzudo, L. Malerba, F. Banhart, W.J. Weber, F. Willaime, S.L. Dudarev, D. Simeone, Improving atomic displacement and replacement calculations with physically realistic damage models, Nat. Commun. 9 (1) (2018) 1084. https://doi.org/10.1038/s41467-018-03415-5

[61] A. Stankovskiy, G. van den Eynde, P. Baeten, C. Trakas, P.M. Demy, L. Villatte, ALEPH2 - A general purpose Monte Carlo depletion code, American Nuclear Society - ANS, United States, United States, 2012. http://inis.iaea.org/search/search.aspx?orig_q=RN:44063527.

[62] A. Konobeyev, U. Fischer, Y. Korovin, S.P. Simakov, Evaluation of effective threshold displacement energies and other data required for the calculation of advanced atomic displacement cross-sections, Nucl. Energy Technol. 3 (2017) 169–175. https://doi.org/10.1016/j.nucet.2017.08.007

[63] D.A. Brown, M.B. Chadwick, R. Capote, A.C. Kahler, A. Trkov, M.W. Herman, A.A. Sonzogni, Y. Danon, A.D. Carlson, M. Dunn, D.L. Smith, G.M. Hale, G. Arbanas, R. Arcilla, C.R. Bates, B. Beck, B. Becker, F. Brown, R.J. Casperson, J. Conlin, D.E. Cullen, M.-A. Descalle, R. Firestone, T. Gaines, K.H. Guber, A.I. Hawari, J. Holmes, T.D. Johnson, T. Kawano, B.C. Kiedrowski, A.J. Koning, S. Kopecky, L. Leal, J.P. Lestone, C. Lubitz, J.I. Márquez Damián, C.M. Mattoon, E.A. McCutchan, S. Mughabghab, P. Navratil, D. Neudecker, G.P.A. Nobre, G. Noguere, M. Paris, M.T. Pigni, A.J. Plompen, B. Pritychenko, V.G. Pronyaev, D. Roubtsov, D. Rochman, P. Romano, P. Schillebeeckx, S. Simakov, M. Sin, I. Sirakov, B. Sleaford, V. Sobes, E.S. Soukhovitskii, I. Stetcu, P. Talou, I. Thompson, S. van der Marck, L. Welser-Sherrill, D. Wiarda, M. White, J.L. Wormald, R.Q. Wright, M. Zerkle, G. Žerovnik, Y. Zhu, et al., ENDF/B-VIII.0: the 8 th major release of the nuclear reaction data library with CIELO-project cross sections, new standards and thermal scattering data, Nucl. Data Sheets 148 (2018) 1–142. https://doi.org/10.1016/j.nds.2018.02.001

[64] A.E. Committee, E399 - 90: Test Method for Linear-Elastic Plane-Strain Fracture Toughness of Metallic Materials. https://doi.org/10.1520/E0399-23

[65] D. Terentyev, J. Riesch, S. Lebediev, T. Khvan, A. Dubinko, A. Bakaeva, et al., Strength and deformation mechanism of tungsten wires exposed to high temperature annealing: impact of potassium doping, Int. J. Refract. Met. Hard Mater. 76 (2018) 226–233. https://doi.org/10.1016/j.ijrmhm.2018.07.002

[66] Y.-L. Liu, H.-B. Zhou, S. Jin, Y. Zhang, G.-H. Lu, et al., Dissolution and diffusion properties of carbon in tungsten, J. Phys. Condens Matter 22 (44) (2010) 445504. https://doi.org/10.1088/0953-8984/22/44/445504

[67] J. Riesch, J.-Y. Buffiere, T. Höschen, M. Di Michiel, M. Scheel, C. Linsmeier, J.H. You, et al., In situ synchrotron tomography estimation of toughening effect by semi-ductile fibre reinforcement in a tungsten-fibre-reinforced tungsten composite system, Acta Mater. 61 (19) (2013) 7060–7071. https://doi.org/10.1016/j.actamat.2013.07.035

[68] J. Riesch, J. Almanstötter, J.W. Coenen, M. Fuhr, H. Gietl, Y. Han, T. Höschen, C. Linsmeier, N. Travitzky, P. Zhao, R. Neu, et al., Properties of drawn W wire used as high performance fibre in tungsten fibre-reinforced tungsten composite, IOP Conf. Ser. Mater. Sci. Eng. 139 (2016) 012043. https://doi.org/10.1088/1757-899X/139/1/012043

[69] D. Terentyev, M. Rieth, G. Pintsuk, A. von Müller, S. Antusch, A. Zinovev, A. Bakaev, K. Poleshchuk, G. Aiello, et al., Effect of neutron irradiation on tensile properties of advanced Cu-based alloys and composites developed for fusion applications, J. Nucl. Mater. 584 (2023) 154587. https://doi.org/10.1016/j.jnucmat.2023.154587

[70] K. Zhang, E. Gaganidze, M. Gorley, et al., Development of the material property handbook and database of CuCrZr, Fusion Eng. Des. 144 (2019) 148–153. https://doi.org/10.1016/j.fusengdes.2019.04.094

[71] S.A. Fabritsiev, A.S. Pokrovsky, Effect of high doses of neutron irradiation on physico-mechanical properties of copper alloys for ITER applications, Fusion Eng. Des. 73 (1) (2005) 19–34. https://doi.org/10.1016/j.fusengdes.2004.12.003

[72] A. Zinovev, D. Terentyev, C.-C. Chang, C. Yin, A. Bakaev, M. Rieth, P. Lied, J. Reiser, C. Bonnekoh, et al., Effect of neutron irradiation on ductility of tungsten foils developed for tungsten-copper laminates, Nucl. Mater. Energy 30 (2022) 101133. https://doi.org/10.1016/j.nme.2022.101133

[73] J. Riesch, A. Feichtmayer, M. Fuhr, J. Almanstötter, J.W. Coenen, H. Gietl, T. Höschen, C. Linsmeier, R. Neu, et al., Tensile behaviour of drawn tungsten wire used in tungsten fibre-reinforced tungsten composites, Phys. Scr. T170 (2017) 014032. https://doi.org/10.1088/1402-4896/aa891d

[74] M. Fuhr, Deformation mechanisms of drawn tungsten wires, Ph.d. thesis, Technische Universität München, München, 2024. https://mediatum.ub.tum.de/?id=1709412.

[75] U.M. Ciucani, L. Haus, H. Gietl, J. Riesch, W. Pantleon, et al., Microstructural evolution in single tungsten fiber-reinforced tungsten composites during annealing: recrystallization and abnormal grain growth, J. Nucl. Mater. 543 (2021) 152579. http://www.sciencedirect.com/science/article/pii/S0022311520311879. https://doi.org/10.1016/j.jnucmat.2020.152579

[76] Y. Mao, J.W. Coenen, A. Terra, L. Gao, A. Kreter, M. Wirtz, C. Liu, C. Chen, J. Riesch, Y. Wu, C. Broeckmann, C. Linsmeier, et al., Demonstrating tungsten fiber-reinforced porous-matrix tungsten composites for future fusion application, Nucl. Fusion 62 (10) (2022) 106029. https://doi.org/10.1088/1741-4326/ac8c55

[77] A. Feichtmayer, J. Riesch, B. Curzadd, T. Höschen, T. Schwarz-Selinger, M. Appel, R. Colson, S. Estermann, R. Lürbke, R. Neu, et al., The general-purpose irradiated fiber and foil experiment for material characterization under fusion-relevant loads, Fusion Eng. Des. 217 (2025) 115114. https://doi.org/10.1016/j.fusengdes.2025.115114